TRIUMF

ANNUAL REPORT
SCIENTIFIC ACTIVITIES
2000

ISSN 1492-417X

CANADA'S NATIONAL LABORATORY
FOR PARTICLE AND NUCLEAR PHYSICS

OPERATED AS A JOINT VENTURE

MEMBERS:

THE UNIVERSITY OF ALBERTA
THE UNIVERSITY OF BRITISH COLUMBIA
CARLETON UNIVERSITY
SIMON FRASER UNIVERSITY
THE UNIVERSITY OF VICTORIA

ASSOCIATE MEMBERS:

THE UNIVERSITY OF MANITOBA
L'UNIVERSITÉ DE MONTRÉAL
QUEEN'S UNIVERSITY
THE UNIVERSITY OF REGINA
THE UNIVERSITY OF TORONTO

UNDER A CONTRIBUTION FROM THE
NATIONAL RESEARCH COUNCIL OF CANADA

OCTOBER 2001

The contributions on individual experiments in this report are outlines intended to demonstrate the extent of scientific activity at TRIUMF during the past year. The outlines are not publications and often contain preliminary results not intended, or not yet ready, for publication. Material from these reports should not be reproduced or quoted without permission from the authors.

Experiment 684
μSR spin relaxation studies of small molecules in the gas phase
(J. Pan, D. Fleming, UBC-TRIUMF)

This experiment studies the muon spin relaxation in some simple gas-phase systems with the primary goal of measuring the chemical reaction rates. Due to the loss of beam time as a result of the cyclotron and the M9 beam line problems, only two days of experiment with reduced beam current were carried out for the study of Mu + CO with N_2 as moderator at room temperature in the longitudinal field (LF).

The motive of this year's experiment is to complete the study of the Mu + CO reaction over a wide range of pressures from 2 to 500 bar in the longitudinal field in order to gain better understanding of the spin rotation relaxation process in μSR experiments in general and in Mu + CO reactions in particular. A better understanding of the collisional relaxation process is in turn helpful for the interpretation of data in terms of the chemical kinetics of the reaction. Particularly, the relaxation rate constants of the Mu + CO reaction measured in transverse field have indicated that the collisional relaxation rate is essentially pressure independent over the pressure range of 2–500 bar.

Unfortunately, the little beam we actually had was not sufficient to investigate the reaction in the LF. We were only able to take about 20 runs, while about 10 runs are required to have a complete field dependence survey for each gas mixture and at least 5–6 gas mixtures are required to cover the relevant pressure range. Needless to say, the data obtained were not sufficient to reach any conclusions.

Experiment 749
Muonium-substituted free radicals
(P.W. Percival, SFU)

Addition of muonium (Mu) to an unsaturated molecule such as an alkene or arene results in a free radical incorporating the muon in place of a proton. According to modern terminology such a radical is termed a muoniated radical, to emphasize the formal replacement of a hydrogen atom by muonium in what is otherwise a recognized chemical structure (cf. a deuterated molecule, which contains D instead of H). In terms of electronic structure there is no difference between the H and Mu analogues (at least, to the level of the Born-Oppenheimer approximation). Isotope effects do exist, of course; they are related to intramolecular motion involving Mu. Thus, increased zero-point vibration in C–Mu bonds, for example, can influence the conformations of organic free radicals and the rates of chemical reactions. In other respects, however, the muoniated radical behaves like its H analogue and the muon can be viewed as a passive spin probe, which allows us to explore chemical and physical properties of the radical that may not otherwise be amenable to experiment.

In Expt. 749 and its predecessors we have applied the muon spin probe to investigate topical and/or fundamental questions in free radical chemistry. One of these is the electronic structure of fullerenyl radicals, specifically the unpaired spin distribution in H (or Mu) adducts of fullerenes. We were able to map unpaired spin densities by determining ^{13}C hyperfine constants by means of muon level-crossing resonance (μLCR) [Percival *et al.*, Chem. Phys. Lett. **245**, 90 (1995)].

Another goal of Expt. 749 has been to understand the factors that influence radical addition to curved polyaromatic hydrocarbons (PAHs), of which fullerenes can be considered "ideal" examples, having closed surfaces constructed from carbon atoms alone. In the case of C_{60}, addition of an H atom or other small radical results in a single radical product, since all carbons are identical. In contrast, the ellipsoidal C_{70} molecule has five chemically inequivalent sets of carbon atoms. In principle, therefore, five distinct radicals could be formed.

Several years ago we investigated C_{70} by using TF-μSR to detect muonium adducts, i.e. isomeric C_{70}Mu radicals, but we were only able to distinguish four isomeric radicals [Addison-Jones *et al.*, Hyp. Int. **86**, 817 (1994)]. They have markedly different abundances, which suggests varying reactivity of the different carbon sites in C_{70}. Since the fifth (missing) radical corresponds to addition of Mu (H) to the "equator" of C_{70}, where the curvature of the carbon network is least, we also investigated the Mu adducts of the flat polyaromatic hydrocarbon pyrene [Percival *et al.*, Can. J. Chem. **77**, 326 (1999)], and a curved variant, 1,8-dioxa[8](2,7)pyrenophane [1999 TRIUMF Annual Report].

During 2000 we extended studies to another PAH, triphenylene, and its partially hydrogenated derivative (Fig. 57). TF-μSR and μLCR spectra of triphenylene

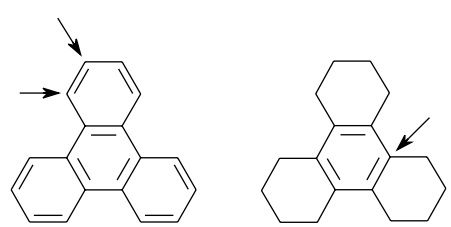

Fig. 57. The chemical structures of triphenylene (left) and dodecahydrotriphenylene (right). TF-μSR and μLCR studies show that Mu adds to these molecules at the positions indicated by the arrows.

revealed the formation of two muoniated radicals, and comparison of the muon and proton hyperfine constants with quantum calculations confirmed our expectation that Mu adds to carbons 1 and 2 (and symmetrical positions in the other benzene rings). These sites are blocked in dodecahydrotriphenylene. Nevertheless, we detected clear signals of a muoniated radical, which can only correspond to addition at the central benzene ring. This is significant because it confirms our view that failure to detect Mu addition at trigonal carbons in other PAHs (including the "equatorial" site in C_{70}) is *not* due to the unreactivity of such sites, but rather to the competition from more reactive sites on the perimeter of the molecules (or more curved areas of C_{70}).

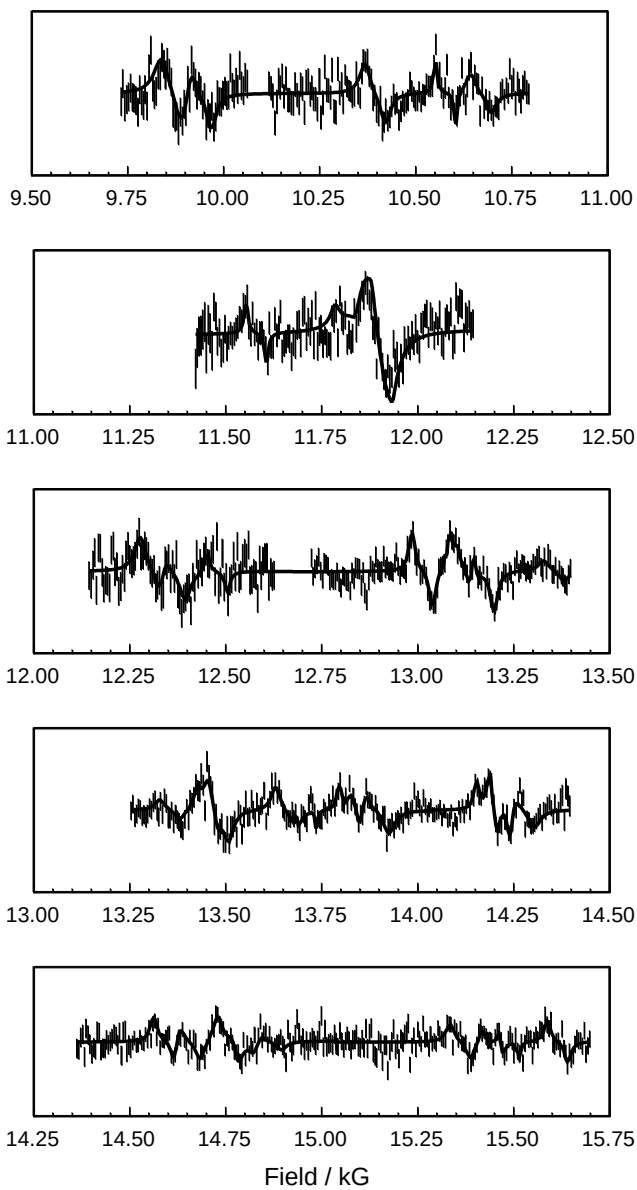

Fig. 58. Segments of the muon level-crossing spectrum obtained from a dilute solution of $^{13}C_{70}$.

Finally, to complete Expt. 749, we returned to an earlier goal, mapping the unpaired spin distribution of the available $C_{70}Mu$ radicals by detecting and assigning the μLCR resonances due to ^{13}C hyperfine constants in $^{13}C_{70}$. This is much more difficult than the earlier study of $^{13}C_{60}$ because of the multiple radical products and the consequent spread of signal intensity and potential overlap of resonances from different isomers. The magnitude of the problem can be gauged from Fig. 58, which shows a compilation of spectra with fitted resonances. Detailed analysis and assignment of signals is under way.

Experiment 768
Generalized FFLO state and anomaly of flux line lattice state in novel superconductors
(R. Kadono, KEK-IMSS; J. Akimitsu, Aoyama Gakuin)

The origin of large hysteresis in the isothermal dc magnetization near the upper critical field H_{c2} (or so-called "peak effect") observed in $CeRu_2$ has been an issue of considerable attention because of the possibility of an associated novel mixed state. Although the peak effect is rather commonly observed in clean type II superconductors and is usually explained by the increase of net pinning force due to the softening of the flux line lattice (FLL) and associated optimization of the vortex configuration along with randomly distributed pinning centres, the one observed in $CeRu_2$ turned out to exhibit an additional feature of field and temperature hysteresis at the onset of the irreversible region. This hysteresis has been interpreted as a manifestation of the first-order phase transition to a further inhomogeneous novel mixed state predicted by Fulde-Ferrel-Larkin-Ovchinnikov (FFLO).

The FFLO state has been predicted to occur in clean type II superconductors (i.e., electronic mean free path l is much longer than the superconducting coherence length ξ_0) with large Pauli paramagnetic spin susceptibility χ_s of the conduction electrons and a large Ginzburg-Landau parameter κ. The system satisfying the latter two conditions can reach the Clogston-Chandrasekhar (CC) limit where the spin polarization (Zeeman) energy $\chi_s H^2/2$ is comparable with the superconducting condensation energy $H_c^2/8\pi$ at fields H near H_{c2}. The recent model including the effect of orbital current predicts that the system near the CC limit falls into a new inhomogeneous state (generalized FFLO state or GFFLO state) at a field H_i below H_{c2} where the order parameter is spatially modulated with periodic planar nodes aligned perpendicular to the vortices. In order to obtain experimental clues to distinguish the origin of FLL softening, the microscopic property of magnetic vortices in the mixed state of a

high-quality $CeRu_2$ crystal has been studied by muon spin rotation (μSR). We note that the sample quality has been much improved from that measured in the earlier μSR experiment, as indicated by the increase of the residual resistivity ratio from 30 to 91.

We have found that the spatial distribution of magnetic induction $\mathbf{B}(\mathbf{r})$ probed by muons is perfectly described by the London model for the triangular vortex lattice with appropriate modifications to incorporate the high-field cutoff around the vortex core and the effect of long-range defects in the vortex lattice structure at lower fields. As shown in Fig. 59, the vortex core radius is proportional to $H^{(\beta-1)/2}$ with $\beta \simeq 0.53$, which is in good agreement with the recently observed nonlinear field dependence of the electronic specific heat coefficient $\gamma \propto H^{\beta}$. In particular, the anomalous increase of magnetic penetration depth in accordance with the peak effect in dc magnetization ($\geq H^* \simeq 3$ T at 2.0 K) has been confirmed (see Fig. 59); this cannot be explained by the conventional pair-breaking effect due to magnetic field. In addition, the spontaneous enhancement of flux pinning, which is also associated with the peak effect, has been demonstrated microscopically. These results strongly suggest the onset of collective pinning induced by a new vortex state having an anomalously enhanced quasiparticle density of states for $H \geq H^*$.

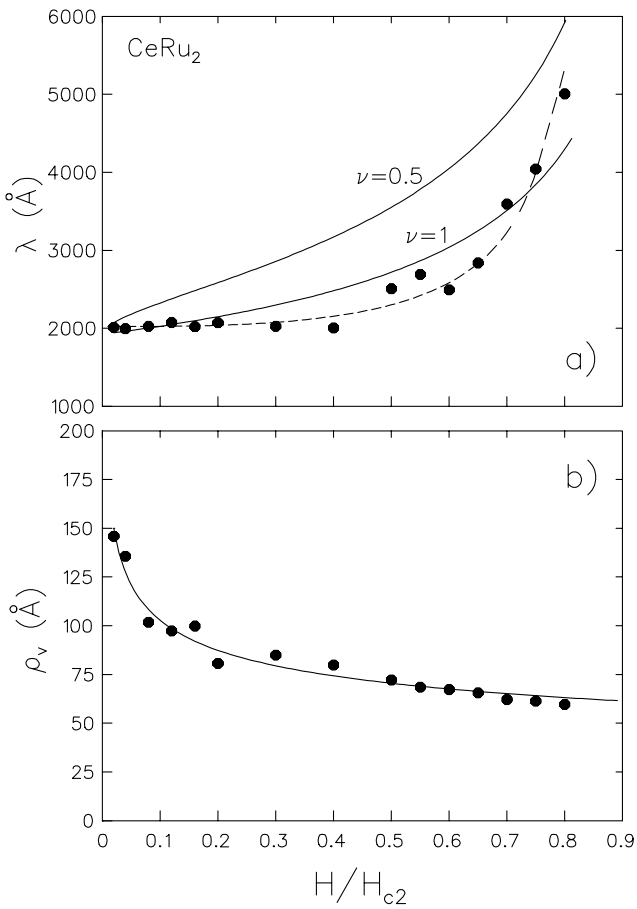

Fig. 59. a) Magnetic penetration depth λ and b) vortex core radius ρ_v vs. field in $CeRu_2$ at 2 K. While λ was obtained by fitting data with the modified London model, ρ_v was determined as a peak of supercurrent density $j(r)$ around the vortex with $j(r)$ calculated directly from $\mathbf{B}(\mathbf{r})$ using Maxwell's relation. Solid curves in a) are calculated by a model (see the forthcoming publication), while the dashed line is a guide for the eye. Fitting the result by a power law is shown in b) as a solid curve.

Experiment 774
Muon charge state dynamics in LPE GaAs
(B. Hitti, S.R. Kreitzman, TRIUMF)

We report on the significant progress achieved to date in understanding the temperature dependence of the various muon states and their dynamics in the technologically important compound semiconductor GaAs. New data were gathered on our high purity LPE samples and their semi-insulating substrate. The new information is used to help unravel the behaviour of muons in the simpler LPE system from that of the less well characterized substrate material. Our results confirm that, at the low dopant concentration where the basic dynamical processes are best revealed, the use of structurally defect free LPE material is essential to study intrinsic processes.

In our previous beam periods the temperature dependence of the final state diamagnetic fraction was measured at 2 kG in a number of samples between 10 and 650 K [see Fig. 75, TRIUMF Annual Report Scientific Activities 1999]. These data clearly identify two regimes where the diamagnetic amplitude as a function of temperature was dramatically different in the LPE and substrate samples. In the low temperature regime (10–100 K), substrate data seemed to display a simple behaviour but lacked the well known double step corresponding to the Mu^0_{BC} ionization. Modelling an electron recapture process, we noticed that the step is not eliminated but significantly suppressed. To clarify this issue we acquired detailed data (Fig. 60) on the substrate at low temperature which clearly shows that a small step is indeed present. At higher temperatures (400–550 K) the LPE behaviour seemed to be infected by features from the substrate. We therefore suspected that about 25% of the low energy muons were penetrating the 200 μm LPE layer and stopping in the substrate. To test this hypothesis the LPE diamagnetic amplitude was re-measured with a 37.5 μm thick Cu degrader to ensure that the muons encountered only LPE material. Under these conditions the suspect high temperature structure indeed vanished (Fig. 61), confirming said hypothesis.

In addition to the radio frequency μSR data described above, transverse field data were obtained on

the diamagnetic and two paramagnetic states of muonium in both the LPE and substrate material. These data confirm the general picture obtained by the radio frequency technique. The model involves the ionization of Mu^0_{BC} at about 100 K, the ionization on Mu^0_T just above room temperature, followed by charge exchange with free electrons from the conduction band above 500 K.

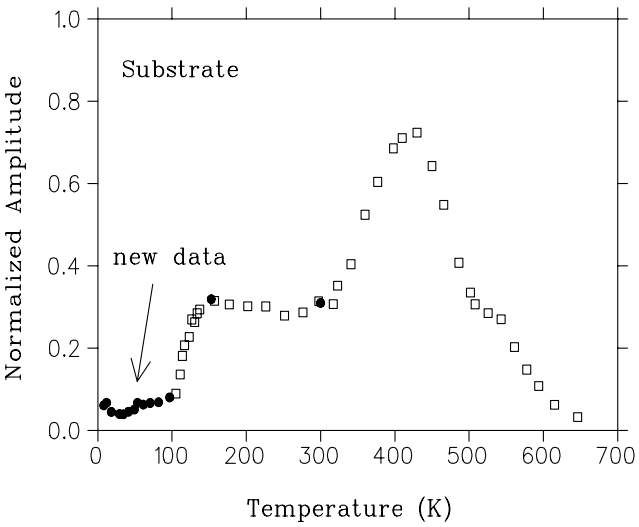

Fig. 60. The diamagnetic amplitude measured in the substrate. Open squares show the previous data and the filled circles show the new data; the small step at 50 K is clearly present.

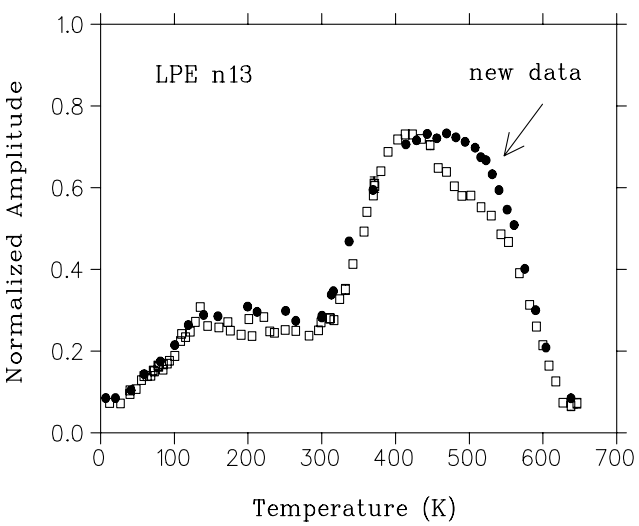

Fig. 61. The diamagnetic amplitude measured in the LPE n13 sample. Open squares show the previous data and the filled circles show the new data. The structure seen previously between 400 K and 550 K is not present in the more recent data.

Experiment 776
Rare-earth materials with disordered spin structures
(D.R. Noakes, Virginia State)

This experiment is a muon spin relaxation (μSR) study of RE-Mg-Zn (RE = rare earth) quasicrystals and PrP_x induced moment "spin glasses", motivated by the common features in the results of Expt. 665 (Al-Mn-Si quasicrystals) and Expt. 640 (low-carrier-density Kondo-lattice CeNiSn and related materials). Study of the rare earth quasicrystals was completed, as described in the 1998 Annual Report. A paper describing the surprising observation of strong-collision-dynamic Lorentzian Kubo-Toyabe relaxation in PrP_x, as discussed in the 1998 and 1999 Annual Reports and presented at the 1999 International Conference on μSR, has appeared in the proceedings of the conference in Physica B. A paper on Monte Carlo simulations of the singlet-ground crystalline electric field level fluctuation model for the observed μSR in PrP_x, described in the 1999 Annual Report, is now in preparation.

Experiment 777
Vortex state of *s*-wave superconductors investigated by muon spin rotation
(A. Price, R. Miller, UBC/TRIUMF)

In Expt. 777, we continued our investigation of the vortex state of conventional superconductors with the three-dimensional superconductors V_3Si and $LuNi_2B_2C$. V_3Si, a cubic superconductor with T_c = 17 K, and $LuNi_2B_2C$, with T_c = 16.6 K, have been extensively investigated with small angle neutron spectroscopy, STM and other methods. Both superconductors show changing vortex lattice geometries as the applied field is increased.

$LuNi_2B_2C$

Transverse field data taken on the M20 beam line on $LuNi_2B_2C$ were analyzed with a field distribution that takes into account non-local effects. Non-local effects in a superconductor arise when the small coherence length London limit no longer applies. This can occur at nodes in the gap in unconventional superconductors or due to strong gap anisotropy, as is the case in $LuNi_2B_2C$. Our analysis confirms the presence of a square vortex lattice at applied fields larger than 2 kOe, as reported by SANS and STM.

Our μSR data indicate that the penetration depth measured by μSR varies considerably with applied magnetic field. This effect has been seen previously in $NbSe_2$ (see previous Expt. 777 Annual Reports), although the magnitude of the field dependence in $LuNi_2B_2C$ is about five times larger (see Fig. 62 top).

The core radius, defined as the distance between

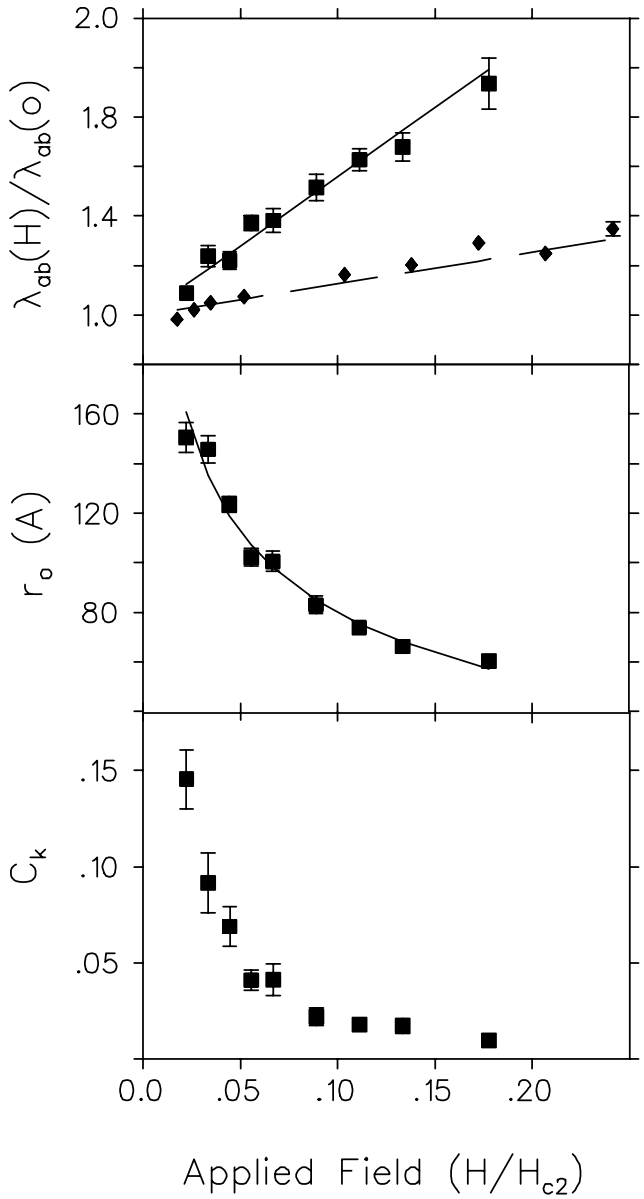

Fig. 62. Magnetic field dependence in $LuNi_2B_2C$ at $T = 2.2$ K of: top) the effective penetration depth, λ_{ab} (squares), and in $NbSe_2$ (diamonds) at $T = 2.4$ K; middle) the vortex core radius in $LuNi_2B_2C$; bottom) fitting parameter c_k.

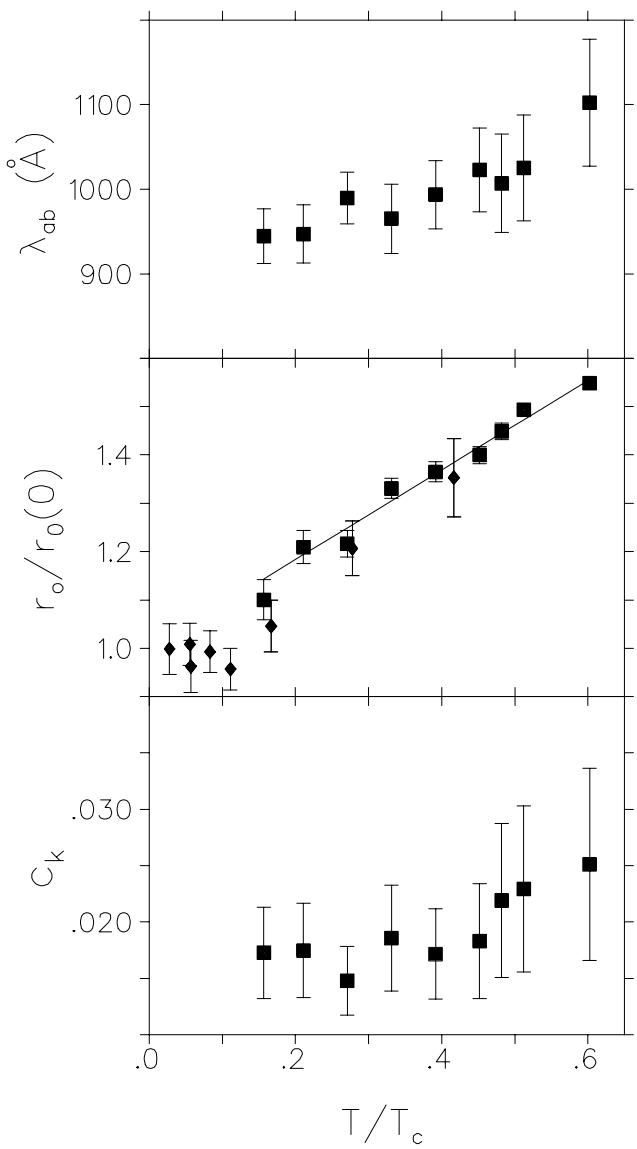

Fig. 63. Temperature dependence in $LuNi_2B_2C$ at $H = 12$ kOe of: top) the effective penetration depth, λ_{ab} (squares); middle) the vortex core radius in $LuNi_2B_2C$ (squares) and in $NbSe_2$ (diamonds) at $H = 5$ kOe; and bottom) fitting parameter c_k.

the vortex core centre and the maximum in the supercurrent, also varies strongly with applied magnetic field. This observation of a magnetic field dependent core radius is the first in a $3D$ superconductor. Previously, μSR measurements reported similar field dependence in $2D$ $NbSe_2$, $YBCO_{6.6}$ and $YBCO_{6.95}$ (see Fig. 62 middle).

Previous Expt. 777 measurements of the vortex core electronic properties of $NbSe_2$ showed that bound quasiparticle states in the vortex core cause the vortex core radius to decrease with decreasing temperature [Miller *et al.*, Phys. Rev. Lett. **85**, 1540 (2000)]. This effect was predicted by Kramer and Pesch in 1974. In $LuNi_2B_2C$, we find a similar effect, shown in Fig. 63. Furthermore, the slope of the core radius as a function of temperature is nearly the same as in $NbSe_2$, indicating the likely presence of bound quasiparticle states in $LuNi_2B_2C$.

V_3Si

Initial μSR measurements of the magnetic field distribution in cubic V_3Si have been made on the M20 beam line, using the MULTI spectrometer. Analyzed with the conventional Ginzburg-Landau field distribution (without non-local effects), the measurements fit relatively well to a hexagonal vortex lattice.

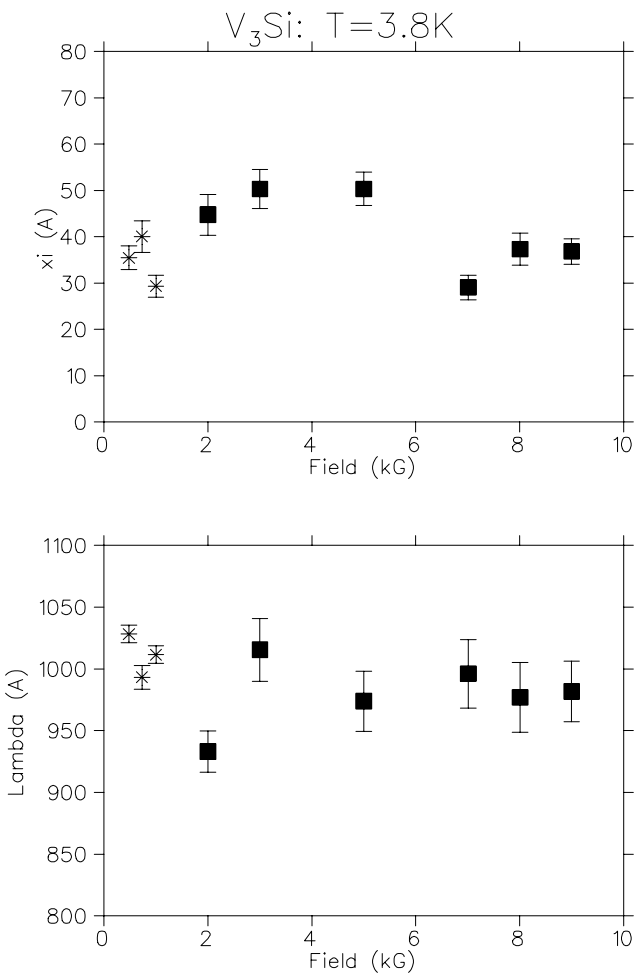

Fig. 64. Magnetic field dependence in V_3Si at $T = 3.8$ K of: top) the effective coherence length, ξ; and bottom) the effective penetration depth, λ_{ab}.

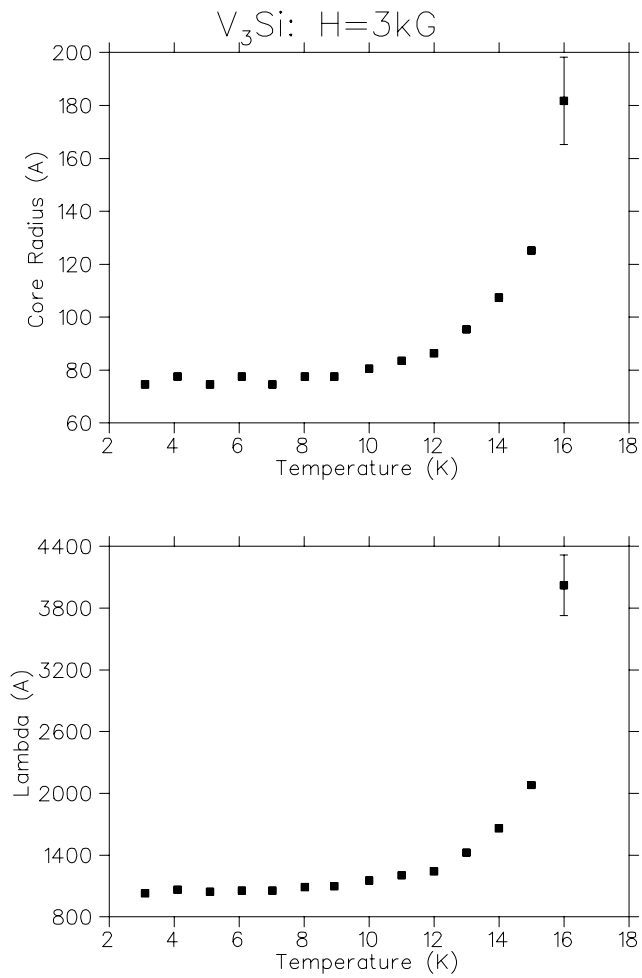

Fig. 65. Temperature dependence in V_3Si at $H = 3$ kOe of: top) the core radius; and bottom) the effective penetration depth, λ_{ab}.

Figure 64 shows the field dependence of the effective coherence length, closely related to the core radius, and of the effective penetration depth. Surprisingly, over this applied field range, neither quantity is dependent on magnetic field, contrary to our earlier measurements. More measurements are planned with a different sample of V_3Si and over an extended magnetic field range.

Finally, Fig. 65 indicates that unlike $NbSe_2$ and $LuNi_2B_2C$, the core radius in V_3Si is not temperature dependent at low temperature and that there is no Kramer-Pesch effect in V_3Si in this temperature range.

Future plans

Because of the surprising absence of either a field dependent core radius or a Kramer-Pesch effect, we plan to repeat the experiment on a different sample of V_3Si. We also plan to investigate the role of Ta doping on the field dependence of the core radius in $NbSe_2$.

Experiment 782
Non-fermi-liquid behaviour and other novel phenomena in heavy-fermion alloys
(D.E. MacLaughlin, California, Riverside)

We have carried out μSR experiments on f-electron heavy-fermion alloys in which deviations from "normal" fermi-liquid heavy-fermion behaviour have been discovered. Thermodynamic and transport measurements indicate that the fermi-liquid description appropriate to a conventional spin-singlet Kondo system does not apply to certain heavy-fermion alloys [i.e. articles in Proc. Conf. on Non-Fermi Liquid Behavior in Metals, Coleman *et al.* eds., J. Phys. Cond. Matter **8** (1996)]. Perhaps the most striking non-fermi-liquid (NFL) low-temperature anomalies are a linear temperature dependence of the resistivity and a logarithmic divergence of the Sommerfeld electronic specific heat coefficient. Both of these properties indicate a serious breakdown of the fermi-liquid picture, and both characterize many NFL heavy-fermion systems discovered

to date.

Evidence has emerged from our μSR and NMR experiments [Bernal *et al.*, Phys. Rev. Lett. **75**, 2023 (1995); Bernal *et al.*, Phys. Rev. **B54**, 13000 (1996); MacLaughlin *et al.*, J. Phys. Cond. Matter **8**, 9855 (1996)] that in some cases this NFL behaviour is due to random disorder in the material. In the simplest disorder-driven picture [MacLaughlin *et al., op. cit.*] this disorder produces an inhomogeneous distribution of Kondo temperatures T_K in the random alloy. Such "Kondo disorder" gives rise to NFL behaviour if a significant fraction of the f spins possess values of T_K lower than the temperature of measurement, in which case these spins are *ipso facto* not in their fermi-liquid ground states. This in turn implies a broad distribution of the heavy-fermion spin polarization, direct signatures of which are correspondingly broad μSR and NMR lines at low temperatures.

Our results have stimulated a considerable amount of theoretical work on disorder-driven mechanisms for NFL behaviour. The Kondo disorder model was put on a firm theoretical footing by Miranda, Dobrosavljević, and Kotliar [J. Phys. Cond. Matter **8**, 9871 (1996)] who found that the effect of structural disorder was enhanced by electron correlation effects. A recent extension of the model by Castro Neto, Castilla, and Jones [Phys. Rev. Lett. **81**, 3531 (1998); Castro Neto and Jones, Phys. Rev. **B62**, 14975 (2000)] takes RKKY interactions between uncompensated spins into account, and predicts NFL behaviour in the form of Griffiths singularities [Phys. Rev. Lett. **23**, 17 (1969)] due to the susceptibilities of RKKY-coupled clusters. Chattopadhyay and Jarrell [Phys. Rev. **B56**, R2920 (1997)] have treated the spin dynamics in the Kondo disorder model, computing the self energy $\Sigma(\omega)$ for distributions of Kondo temperatures including that of Bernal *et al.* [*op. cit.*]. The corresponding low-temperature optical conductivity shows a low-frequency pseudogap, a negative optical mass enhancement, and a linear-in-frequency transport scattering rate, consistent with experimental results in $Y_{1-x}U_xPd_3$ and $UCu_{5-x}Pd_x$.

During the year we carried out μSR studies of two NFL systems at TRIUMF: single-crystal $Ce(Ru_{0.5}Rh_{0.5})_2Si_2$, and $UCu_{5-x}Pt_x$. In the latter we find no evidence for disorder-driven NFL behaviour; this is surprising, given that the isostructural NFL system $UCu_{5-x}Pd_x$ exhibits strong disorder [Bernal *et al., op. cit.*]. In contrast, μSR Knight shifts and linewidths in $Ce(Ru_{0.5}Rh_{0.5})_2Si_2$ are consistent with disorder-driven NFL behaviour, as was also concluded from previous studies [Graf *et al.*, Phys. Rev. Lett. **78**, 3769 (1997); Liu *et al.*, Phys. Rev. **B61**, 432 (2000)]. Our investigations of these and other NFL materials are continuing.

$Ce(Ru_{0.5}Rh_{0.5})_2Si_2$

This NFL alloy had previously been identified as possessing a disorder-driven NFL mechanism from thermodynamic measurements [Graf *et al., op. cit.*] and a ^{29}Si NMR study [Liu *et al., op. cit.*]. But these NMR experiments were carried out in powder samples. The possibility has been raised [Taniguchi *et al.*, J. Phys. Soc. Jpn. **68**, 2026 (1999)] that disorder introduced in the powdering process, or possibly in the original fabrication of the sample, was responsible for the NMR results, and that the mechanism for NFL behaviour in this system is not driven by disorder. We therefore obtained an extremely well-characterized single-crystal sample of $Ce(Ru_{0.5}Rh_{0.5})_2Si_2$ from the group of Y. Myako at Osaka University. NMR on single crystals is difficult due to the small skin depth for radio frequency signals, but no such problem exists for μSR. Furthermore, the NMR experiment used field-aligned epoxy-potted samples, which would not be suitable for μSR because a large fraction of the muons would stop in the epoxy. The single crystal $Ce(Ru_{0.5}Rh_{0.5})_2Si_2$ sample was therefore ideal for a μSR study.

The primary signature of disorder-driven NFL behaviour in TF-μSR is a linewidth which grows faster with decreasing temperature than the bulk susceptibility (or, equivalently, the positive-muon (μ^+) Knight shift). A convenient way to see this behaviour, motivated by the standard Clogston-Jaccarino plot in NMR, is to plot the dimensionless ratio $\delta K(T)/K(T)$ versus the bulk susceptibility $\chi(T)$, with temperature T an implicit parameter. Here $\delta K(T)$ is the rms spread in Knight shifts responsible for the linewidth, and $K(T)$ is the average Knight shift. In a simple heuristic model of disorder-driven NFL behaviour [MacLaughlin, J. Phys. Soc. Jpn. **69**, 33 (2000)] $K(T) \propto \chi(T)$ whereas $\delta K(T) \propto \chi^2(T)$, so that $\delta K(T)/K(T) \propto \chi(T)$.

Preliminary results from our data for $Ce(Ru_{0.5}Rh_{0.5})_2Si_2$, taken with applied field parallel to the c axis of the tetragonal lattice, are shown in Fig. 66. The data bear a striking resemblance to the NMR results [Liu *et al., op. cit.*]; both exhibit a marked increase with increasing susceptibility (decreasing temperature). This strongly indicates that the previously-observed disorder was not an artifact of the particular sample used in the NMR study.

Analysis of our results is not complete, but the data qualitatively confirm that strong disorder in the magnetic susceptibility is present, thus giving evidence for intrinsic structural disorder as a major factor in the NFL properties of $Ce(Ru_{0.5}Rh_{0.5})_2Si_2$. A paper on these results is in preparation.

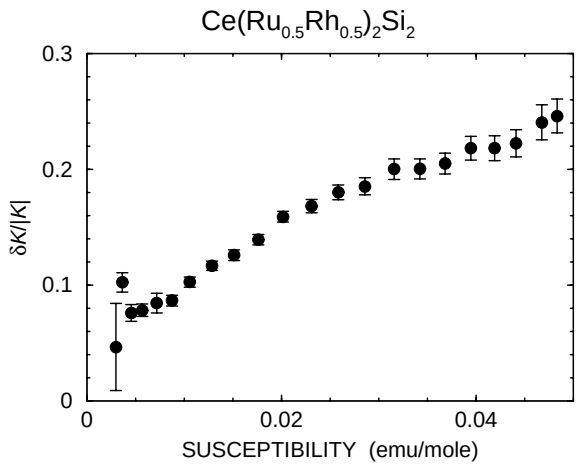

Fig. 66. Dependence of fractional width $\delta K/K$ of μ^+ Knight shift distribution on bulk susceptibility χ, with temperature an implicit parameter, in $Ce(Ru_{0.5}Rh_{0.5})_2Si_2$.

NFL behaviour in $UCu_{5-x}Pt_x$: return to a fermi-liquid?

The alloy system $UCu_{5-x}Pt_x$ is isostructural to $UCu_{5-x}Pd_x$ for $x \lesssim 2.5$ and, like $UCu_{5-x}Pd_x$, exhibits NFL behaviour near $x = 1$ [Chau and Maple, J. Phys. Cond. Matter **8**, 9939 (1996)]. A marked difference between the two systems is found for $x \gtrsim 1.5$, however: $UCu_{5-x}Pd_x$ has a spin-glass phase for $x \gtrsim 2$, whereas $UCu_{5-x}Pt_x$ exhibits fermi-liquid behaviour and no magnetic order [Chau, Ph.D. dissertation, Univ. of California, San Diego (1997)]. This curious behaviour raises questions concerning the role of disorder in the NFL properties of $UCu_{5-x}Pt_x$. Is chemical disorder relevant in this alloy series? Is the loss of NFL behaviour for $x > 1$ related to a QCP at $x = 1$, or is the effect of disorder reduced for some reason?

We have begun TF-μSR studies of this system at TRIUMF. Very preliminary results over the temperature range 2–300 K show considerable differences between μSR spectra of $UCu_{5-x}Pt_x$ and $UCu_{5-x}Pd_x$.

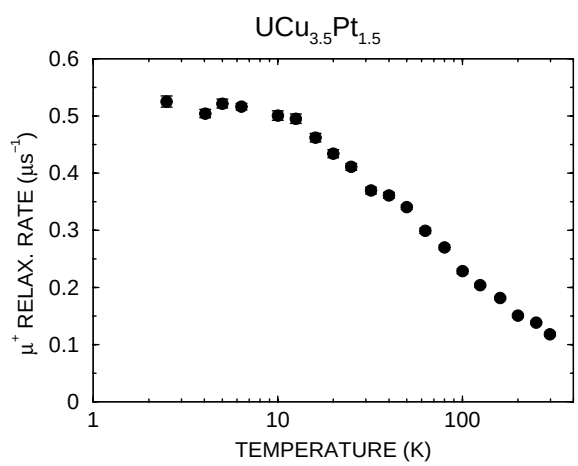

Fig. 67. Temperature dependence of μ^+ Gaussian relaxation rate $\sigma(T)$ in $UCu_{3.5}Pt_{1.5}$. Applied field $H = 10$ kOe.

Figure 67 shows the temperature dependence of the Gaussian width $\sigma(T)$ of the μSR line in $UCu_{3.5}Pt_{1.5}$. Very generally $\sigma(T)/2\pi$ is the rms width of the μ^+ resonance line. At low temperatures $\sigma(T)$ is a factor of six smaller than in $UCu_{5-x}Pd_x$ [Bernal *et al., op. cit.*], which indicates clearly that disorder is not a dominant factor in these alloys.

Experiment 783
Paramagnetic frequency shifts in unconventional superconductors
(R.H. Heffner, LANL; J.E. Sonier, SFU)

$U_{0.965}Th_{0.035}Be_{13}$

In December, 1999 we carried out μ^+ Knight shift measurements in the heavy-fermion superconductor $U_{0.965}Th_{0.035}Be_{13}$ using the dilution refrigerator on the M15 beam line (see Fig. 68). This compound has two superconducting transitions, $T_{c1} = 0.47(5)$ K and $T_{c2} = 0.35(2)$ K, as indicated by heat capacity measurements. There were two key findings in this study:

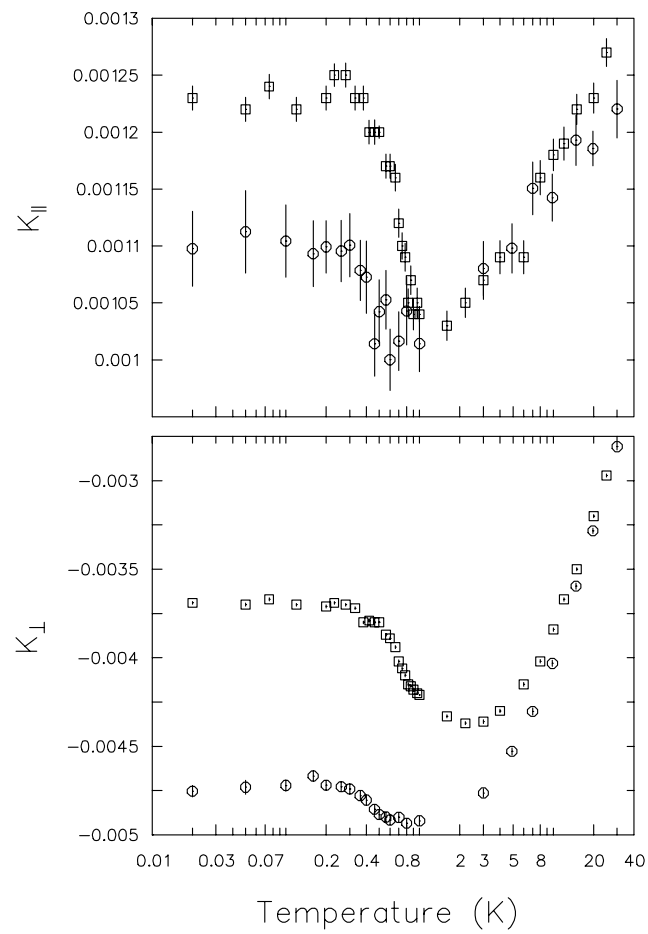

Fig. 68. Temperature dependence of the μ^+ Knight shift K in UBe_{13} (squares) and $U_{0.965}Th_{0.035}Be_{13}$ (circles) measured in an applied magnetic field $H = 10$ kOe. The subscripts $\parallel$ and $\perp$ correspond to two different muon sites.

- In the normal state we observed an anisotropic temperature dependent transferred hyperfine coupling between the μ^+-spin and the U $5f$ electrons.
- An abrupt reduction of χ_s was observed below T_{c1}, whereas χ_s did not change with temperature below T_{c2}.

The first finding is highly unusual, since the contact hyperfine interaction A_c generally involves the s orbitals around the μ^+. The observed anisotropy suggests an admixture of the f and s states, although no definite conclusion has yet been made to explain this result.

The temperature dependence of χ_s shows a sharp drop in χ_s below T_{c1}, indicating that the first superconducting phase consists of Cooper pairs possessing a substate of opposite spin projection (i.e. $S_z = 0$). This state could be of either even or odd parity. There is a clear change in the T-dependence of χ_s below T_{c2}, indicating a change in the superconducting order parameter. The T-independent behaviour is consistent with the development of a multi-component order parameter.

UBe_{13}

In October we performed similar μ^+ Knight shift measurements in pure UBe_{13} crystals. Unlike the Th-doped compound described above, only one superconducting transition at $T_c = 0.87(3)$ K is observed in heat capacity measurements. However, very little is known about this superconducting phase. A preliminary analysis of the Knight shift measurements (Fig. 68) shows that the superconducting phase of UBe_{13} is similar to the first superconducting phase observed in $U_{0.965}Th_{0.035}Be_{13}$; i.e., χ_s decreases as the temperature is reduced. However, unlike the Th-doped compound, the decrease of χ_s continues to $T = 0$ K. The ratio χ_s/χ_n at $T = 0$ K appears to be the same as what would be observed in $U_{0.965}Th_{0.035}Be_{13}$ if the second superconducting phase did not form.

We also observed the onset of an anisotropic transferred hyperfine coupling in the normal state of UBe_{13}. This indicates that the Th impurities are not responsible for this yet unexplained feature.

Present status of Expt. 783

The above observations suggest the possible existence of a multi-component order parameter in $U_{1-x}Th_xBe_{13}$. However, the information gathered so far is not sufficient to decisively identify the superconducting order parameter in either the Th-doped or the pure compound. Thus, we plan to carry out additional Knight shift measurements in 2001 to further address this important issue.

Experiment 784
μSR studies of spin-singlet states in oxides
(A. Fukaya, Y.J. Uemura, Columbia)

In low dimensional Heisenberg antiferromagnetic systems, quantum effects play an important role in macroscopic properties. The ground state may not be a long range Néel ordered state but a singlet state, as observed in Haldane-gap and spin-ladder systems. To study the ground state and spin dynamics of low dimensional quantum spin systems, we have performed comprehensive muon spin relaxation (μSR) studies. We have measured μSR for various oxides: charge ordered system NaV_2O_5, two dimensional (2D) plaquette spin system CaV_4O_9, two-leg ladder system $Sr(Cu,Zn)_2O_3$, and others, and have obtained interesting results. In this report we describe the result of μSR measurements of the 2D quantum system $SrCu_2(BO_3)_2$.

2D quantum systems are quite interesting from the viewpoints of both magnetism and superconductivity. $SrCu_2(BO_3)_2$ is one of only a few 2D compounds with a singlet ground state. Theoretical and experimental studies have clarified that the ground state is an exact singlet dimer state, but it is extremely close to a quantum critical point. This system has a built-in geometrical spin frustration. These features are directly comparable to the case of high-T_c cuprate systems. Thus, $SrCu_2(BO_3)_2$ is a unique 2D spin system which can possibly provide insights for a general understanding of how gapped (spin gap/superconducting) ground states coexist/compete with or cross over to ungapped ground states with/without magnetic order.

We show the temperature dependence of the time spectrum at zero-field (ZF) in Fig. 69. As the temperature decreases, the relaxation becomes fast. Thus, we

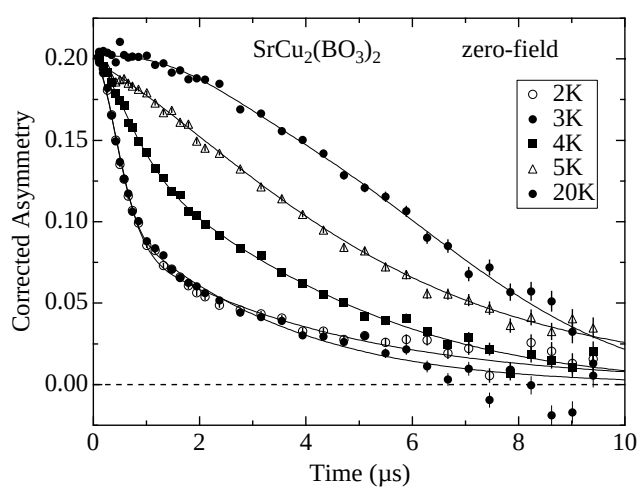

Fig. 69. Temperature dependence of the time spectrum in ZF for $SrCu_2(BO_3)_2$. An unexpected enhancement of relaxation is observed at low temperatures.

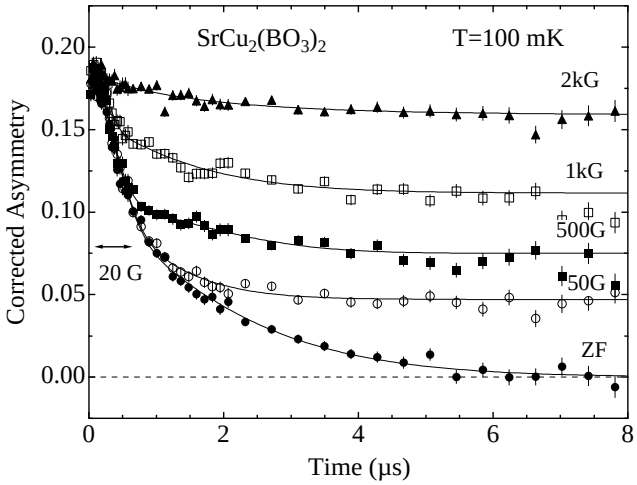

Fig. 70. LF dependence of the time spectrum in $SrCu_2(BO_3)_2$ at 100 mK. The decoupling field is ∼10 times larger than that expected from ZF measurement.

see the existence of some magnetically active spins in a nominally pure spin gap compound at low temperatures. Since the ground state is non-magnetic, muon spins should not relax at low temperatures. Since the μSR method is quite sensitive to small magnetic moments, μSR might detect intrinsic magnetic properties of samples which cannot be detected by other methods. The origin of the anomalous spin freezing, however, has not yet been clarified.

The longitudinal field (LF) dependence of the time spectrum is also quite anomalous. We show the LF dependence at 100 mK in Fig. 70. When a longitudinal field is applied, the asymmetry of the long time tail increases and does not relax. This fact suggests that the local field is static. If the local field is static and has a Gaussian distribution with width Δ, Δ is estimated to be ∼20 G from the time spectrum at early time in zero field. A local field of ∼20 G should be completely decoupled by LF∼200 G. However, even at 2 kG, the time spectrum still shows relaxation. This anomalous relaxation has been termed "undecoupleable Gaussian" relaxation, and has been observed in several systems with geometrically frustrated exchange interactions. Examples of such systems are $SrCr_8Ga_4O_{19}$, Cr-jarosite, $CePt_2Sn_2$, as well as the 1D spin system Y_2BaNiO_5 with charge doping. The details of this line shape, however, are yet to be understood.

Experiment 791
Electronic structure and dynamics of charged muonium centres in semiconductors
(K.H. Chow, B. Hitti, R.F. Kiefl, UBC/TRIUMF)

Results of experiments on muonium are generally considered to be the main source of information on *isolated* hydrogen in semiconductors. Hydrogen is an important impurity which can dramatically affect the electrical and optical properties of these technologically relevant materials. Recently, we unambiguously observed the reaction of Mu^+ with an intentional dopant in a semiconductor. This was the first microscopic study, "as-it-happens", of the formation of a hydrogen or hydrogen-like complex with an intentional dopant in a semiconductor. An important extension of these studies is the characterization of the electronic structure of the isolated precursor state. Such information is interesting for several reasons. First, it enables comparisons with the many theoretical calculations on the subject, which generally locate it at or near a distorted bond-centre position. Thus far, there has been no experimental information on the stucture of H^+ or Mu^+ in a semiconductor. Second, information on the isolated state is an integral part of understanding how the muon or hydrogen makes a transition from its precursor configuration to being part of a complex.

Structural information on a diamagnetic centre such as Mu^+ is obtained by studying the muon-induced and dipolar interactions with the host Ga and As nuclei, all of which have spin 3/2. The most powerful technique for this purpose is μLCR. Recall that a dip in the integrated polarization appears at values of $\mathbf{B}$ where resonant cross-relaxation between the muon and neighbouring nuclear spins occur due to avoided level-crossings in the combined energy levels. The positions of the resonances associated with a particular nucleus are determined by Q and θ, often giving a distinct fingerprint that identifies the neighbouring nucleus and its symmetry. Recall that Q is the strength of the quadrupole interaction and θ is the angle between the applied magnetic field and the muon-nucleus direction. A rough estimate of Q, and hence the position of the resonances, can also be obtained by studying the relaxation of the TF-μSR precession signal as a function of magnetic field. We have performed such an experiment prior to our μLCR experiments to help define a search region.

Our μLCR experiment with $\mathbf{B}||\langle 100\rangle$ in a heavily doped p-type GaAs:Zn sample at 50 K is shown in Fig. 71a. These are the only two resonances visible from 1.7 kG to 3.6 kG, the magnetic field region that we have investigated thus far. This doublet signal can be unambiguously assigned to a nearby Ga atom because the ratio of their positions is identical to the ratio of the ^{69}Ga and ^{71}Ga quadrupole moments (0.168×10^{-24} e.cm^2 and 0.106×10^{-24} e.cm^2). This is further confirmed by Fig. 71b, which shows theoretically the expected resonances. A single value of the electric field gradient was used to produce this figure. (Note that for each isotope, the signal-to-noise is too low to resolve the weaker of the pair.) The unambiguous identification of Ga as being a nearest neighbour of Mu^+ is certainly an

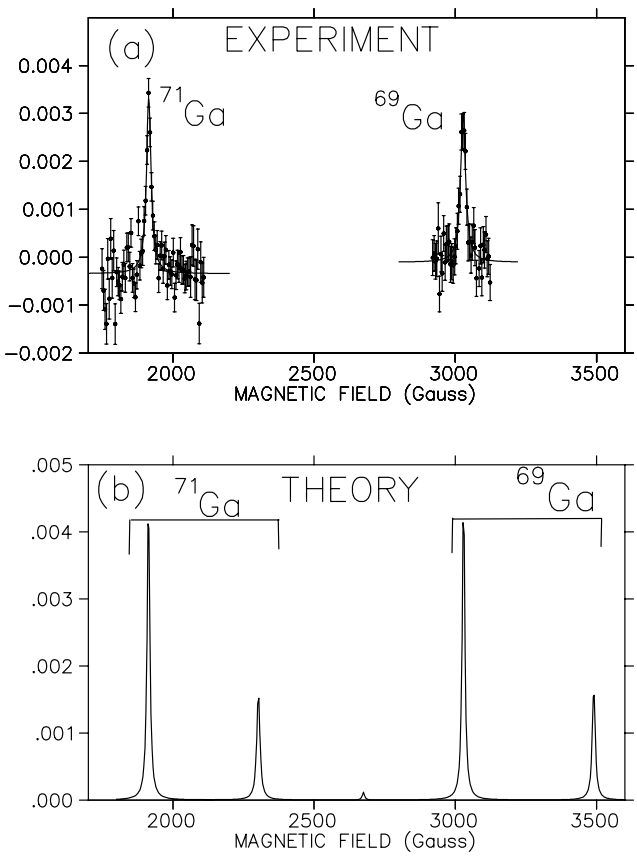

Fig. 71. (a) μLCR at 50 K in heavily doped p-type GaAs:Zn with $\mathbf{B}||\langle 100\rangle$. (b) Theoretical calculation as described in the text.

important step. However, there is nothing in Fig. 71a which tells us its symmetry. This information is obtained by performing a μLCR experiment at another orientation: we have selected $\mathbf{B}||\langle 110\rangle$. The positions and strengths of the lines in Fig. 71a change in a manner that unambiguously confirms that the muon and the Ga nucleus lie on the same $\langle 111\rangle$ axis (i.e. $\theta = 54.7°$).

Thus, all our results are consistent with Mu^+ being located near the centre of a Ga–As bond. However, since we have detected and characterized the Ga only, the picture is still incomplete. Unambiguous proof of the location will only be possible if we can also detect the ^{75}As nucleus and verify that it too has "$\langle 111\rangle$ symmetry". The corresponding resonances are expected to be located at higher magnetic fields, and experiments to locate them are currently being organized.

Experiment 804
Muonium in gallium nitride
(R.L. Lichti, Texas Tech)

The primary goal of Expt. 804 has been to investigate the muonium analogue of hydrogen defect states in GaN and other group-III nitrides. During the past year we obtained the full temperature dependence of the QLCR resonances for a partially compensated Zn-doped GaN sample and for AlN. These data represent static diamagnetic Mu^+ or Mu^- defect centres in these materials. The likely stable sites for these centres are anti-bonding locations oriented into the channels formed by the c-axis stacking order of the Wurtzite structure with Mu^+ associated with nitrogen and Mu^- with the group-III atom (Ga or Al). These sites have the bond oriented at 70° to the c-axis and are commonly noted as $AB_\perp$. Other likely sites are metastable; a second antibonding location with Mu inside the most tightly confined region of the structure and the bond along the c-axis ($AB_\parallel$) and for Mu^+ either of the two bond centred locations ($BC_\perp$ or $BC_\parallel$). QLCR resonances can identify these various sites when the muonium impurity is static. Any Ga related features will have two nearly identical sets of lines with a position ratio of 1.59 due to the two I = 3/2 Ga isotopes, while N related features will reflect a single I = 1 isotope. A single line per isotope only occurs if the bond (and electric field gradient) lies parallel to the applied field, which was along the c-axis of our highly-oriented, thick-film samples. The onset of diffusive motion for $Mu^\pm$, or a slow transition out of a given state, results in broadening of the spectral lines with the resonances disappearing for rapid dynamics in either case. When motion is rapid but highly localized, ie. involving a very few sites, QLCR spectra can still be observed.

Figure 72 shows typical QLCR data for AlN. This spectrum appears to be essentially unchanged up to roughly 850 K, above which the effects of dynamics are seen, but the QLCR is still visible at 1100 K. This single main line is associated with N and almost certainly represents a metastable Mu^+ with a Mu–N bond along the c-axis; we have therefore assigned the line centred at 42 G to the $AB_\parallel$[N] site for Mu^+ in AlN. There is a

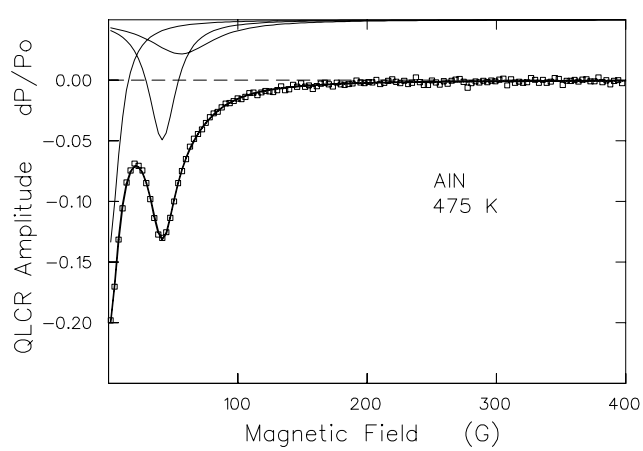

Fig. 72. Raw QLCR data for AlN at 475 K. Main spectrum is a single line centred at 42 G and is assigned to Mu^+ at an $AB_\parallel$[N] site. The broader line at higher field is also from a nitrogen neighbour but represents a second state.

smaller and broader line centred at about 70 G underlying the main resonance; this line is not yet assigned, but no partner has been located. Initial fits suggest a slightly different temperature dependence for the two observed QLCR lines in AlN, with the 70 G line broadening at a slightly lower temperature.

A fit to the QLCR spectra for GaN:Zn in one of the transition regions is shown in Fig. 73 after removal of the non-resonant zero-field feature. Three different states are identified in this spectra. The expected stable $AB_{\perp}$[Ga] site for Mu^- gives two lines per Ga isotope and is subsequently labelled Ga[70°]. The metastable $AB_{\parallel}$[Ga] site for Mu^- has a single strong line per isotope and is labelled as Ga[0°], while the metastable $AB_{\parallel}$[N] location for Mu^+ yields the line labelled N[0°]. Because these various spectra overlap significantly, fits were accomplished by a free parameter fit to the higher field ^{69}Ga lines with parameters for the ^{71}Ga partners forced to values expected from isotope ratios of natural abundances, and the quadrupole and dipole moments. Any remaining feature in the lower field region near 100 G was then fit with parameters free and assigned to an N related resonance; this was always a single dominant line. Numerous other small lines are present and may be from more distant neighbours or other possible sites; however, correlations among these weak signals and assignments have not yet been worked out.

The full temperature dependences for the QLCR linewidths and amplitudes from these fits are displayed in Fig. 74 and the resulting signal intensities along with a fit for each identified state are shown in Fig. 75. In addition to the three states seen in QLCR there is a fourth diamagnetic state which appears in zero-field relaxation measurements (ISIS data) and is tentatively associated with a mobile Mu^+ in the channel region

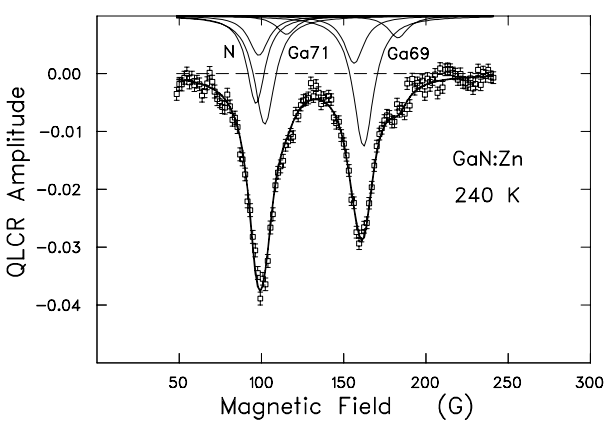

Fig. 73. Fit to QLCR spectra for the GaN:Zn sample in the region where lines from all three observed states have similar amplitudes. Ga assignments are a strong line per isotope from the stable Mu^- and weaker doublet from the metastable Mu^-; the N line is from a metastable Mu^+.

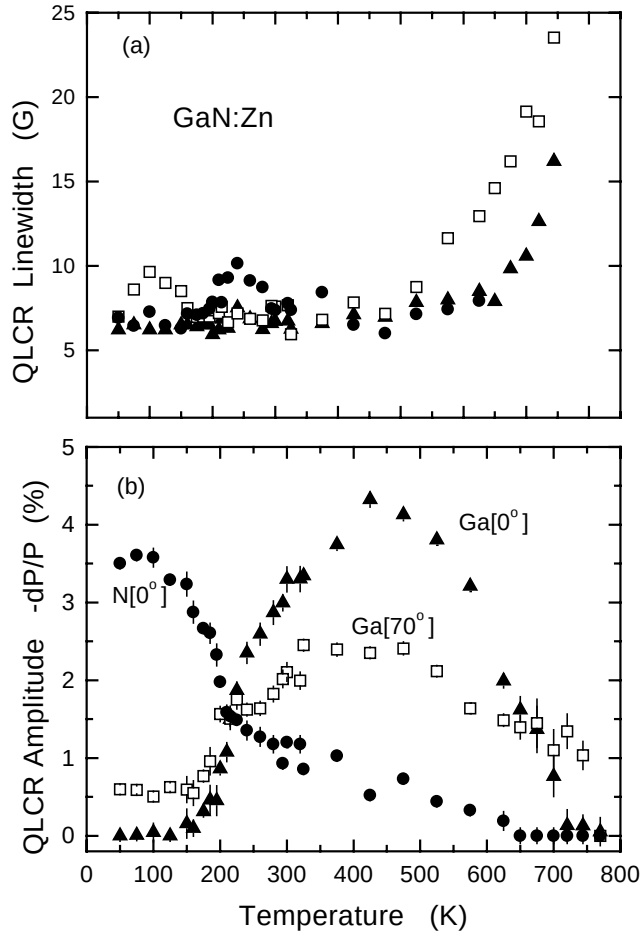

Fig. 74. The temperature dependent linewidths (a) and amplitudes (b) from fits to QLCR spectra for GaN:Zn. Three diamagnetic Mu states are identified: the stable (Ga[70°]) and metastable (Ga[0°]) Mu^- centres, and a metastable Mu^+ centre (N[0°]).

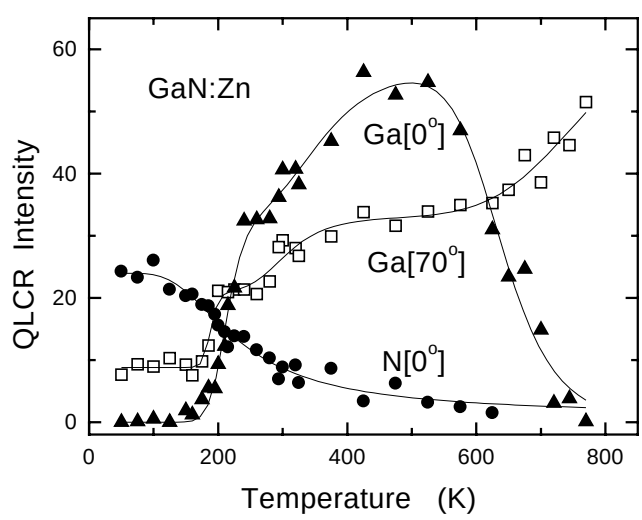

Fig. 75. Temperature dependent QLCR intensities (spectral area) for the compensated GaN:Zn sample. The general picture of the transitions and motion of stable Mu^- centres from these data is consistent with that from ZF relaxation results on more strongly n-type samples.

of the Wurtzite structure. Mu^0 states are also present, representing 30–40% of the muons at low to intermediate temperatures, having atomic-like hyperfine characteristics but with rapid dynamic relaxation based on decoupling curves (ISIS data).

The amplitudes displayed in Fig. 74b show a transition region near 200 K in which the charge state changes from positive to negative. This must presumably involve some Mu^0 centre as an intermediate state. Both the QLCR and ZF relaxation data imply multiple transitions in this region, with more than one site for the Mu^- final state. The amplitudes for the N[0°] signal seem to suggest two separate processes for the transition out of the metastable Mu^+ state; however, the intensity curve (Fig. 75) fits well to a single process. Consistency between the various data sets is poor for parameters related to the state changes near 200 K, thus a detailed model of the dynamics is not yet possible. The general picture of a switch from mostly Mu^+ states at low temperatures to predominantly Mu^- states above 200 K is the same for all of the (n-type) GaN samples we have studied.

The higher temperature dynamics are generally more consistent across various data sets and samples. The stable Mu^- states show diffusive motion above 500 K, which we model as hopping among $AB_\perp$[Ga] sites within the Wurtzite channels. This is indicated in the QLCR data as an increase in the linewidth but no decrease in total intensity for the Ga[70°] QLCR spectrum. Above roughly 650 K the metastable Mu^- state shows a transition into this mobile Mu^- as an increase in the Ga[0°] width accompanied by a decrease in intensity for that spectrum and a net increase in QLCR intensity for the more stable mobile state. The precise energies obtained from different data sets vary for both of these processes but are far more consistent than for the 200 K region. The overall general picture of transitions and motion of the diamagnetic $Mu^\pm$ states in GaN remains the same for all samples studied.

Experiment 814
μSR studies of unconventional superconductivity in Sr_2RuO_4
(G.M. Luke, McMaster)

Since the discovery of high temperature superconductivity in $La_{2-x}Ba_xCuO_4$ there has been an immense effort in all aspects of superconductivity. In addition to searches for higher T_c in studies of various cuprates with different structures and numbers of CuO_2 planes/unit cell, there have been great efforts to search for superconductivity in oxides without Cu. In 1994, Maeno *et al.* discovered superconductivity with $T_c = 1.5$ K in stoichiometric Sr_2RuO_4, which is isostructural to La_2CuO_4.

Many of the properties of Sr_2RuO_4 indicate that its superconducting state is of an unconventional nature. For example, the transition temperature is extremely sensitive to even non-magnetic impurities, and no Hebel-Slichter peak is seen in measurements of the NQR $1/T_1$. ^{17}O NMR measurements observed no change in the Knight shift below T_c, behaviour characteristic of p-wave pairing. We performed zero field muon spin relaxation (ZF-μSR) measurements under Expt. 814 and observed a spontaneous magnetic field below T_c; our results [Luke *et al.*, Nature **394**, 558 (1998)] demonstrated that the superconducting state in Sr_2RuO_4 is characterized by broken time reversal symmetry.

Since our initial ZF-μSR study we have performed measurements on an additional sample with a reduced $T_c = 1.1$ K, in order to confirm that the spontaneous magnetic field onsets at the superconducting T_c. A preliminary account of some of these data has been reported [Luke *et al.*, Physica **B289-290**, 373 (2000)] in a conference proceedings. We have fit the ZF data to the relaxation function given in equation 1 which is appropriate for a local field distribution consisting of a combination of Gaussian (to account for static nuclear dipole moments) and Lorentzian (due to the static internal field associated with the broken time reversal state) components. Equation 1 exhibits a long-time tail of 1/3 (required for any static combination of random internal fields) and reduces to the Gaussian or Lorentzian Kubo-Toyabe forms in the appropriate limits.

$$\mathcal{P}_\mu = \frac{1}{3}+\frac{2}{3}\left[1-(\Delta t)^2 - at\right]\exp\left[-\frac{1}{2}(\Delta t)^2 - at\right]. \quad (1)$$

The Gaussian relaxation rates were held constant for each sample to a value obtained from fitting several runs simultaneously ($\Delta \approx 0.03\ \mu s^{-1}$). We plot the Lorentzian field strength (a) for samples with $T_c = 1.48,\ 1.1$ K in Fig. 76. We see that, within our resolution, the static field onsets at T_c for each sample. This provides additional evidence that the source of the field is the broken time-reversal symmetry superconducting state, rather than some magnetic spin freezing unconnected with superconductivity.

In the mixed state of a type-II superconductor, magnetic flux penetrates the sample in the form of quantized vortices. These vortices repel each other and therefore form a lattice. In most materials the resulting lattice is triangular, although the energy difference between square and triangular lattices is quite small. Square vortex lattices, which can arise from nonlocal effects, have been observed over narrow ranges of magnetic field in niobium and the borocarbides; the

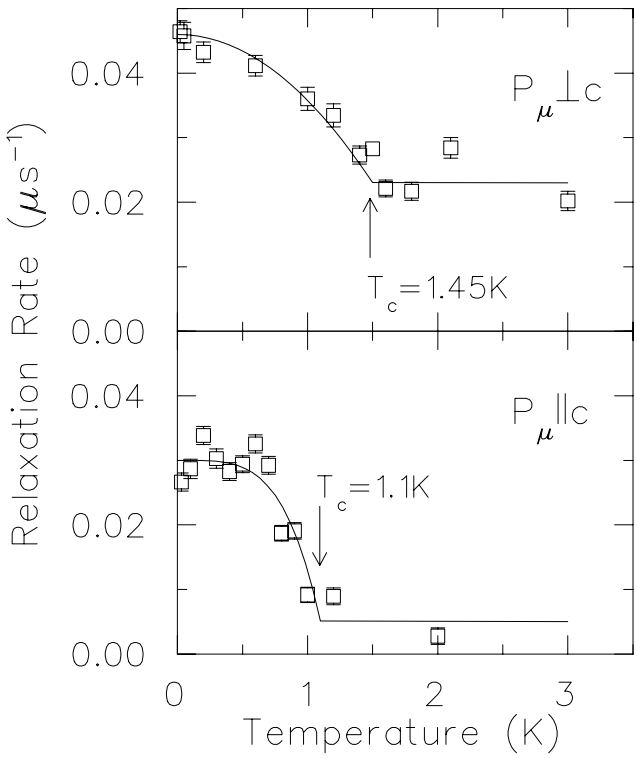

Fig. 76. Lorentzian relaxation rate measured in two samples of Sr_2RuO_4 with superconducting T_c's of 1.45 K and 1.1 K, respectively. Lines are guides to the eye.

observation of a square lattice is not by itself an indication of unconventional superconductivity. However, a prediction of a Ginzburg Landau model for the E_u state in Sr_2RuO_4 is that the Fermi surface geometry should give preferred directions for supercurrent flow within the basal plane, resulting in non-circular vortices. As a result, the vortex lattice should be square for a wide range of field and temperature. A square flux lattice was inferred from μSR measurements and then conclusively observed in neutron diffraction measurements over a wide range of temperature and field.

The presence of a vortex lattice results in a distribution of magnetic fields throughout the specimen; the shape of the field distribution depends on the lattice geometry. In a transverse field (TF-μSR) measurement, muons are implanted throughout the vortex lattice and sample the entire field distribution. A Fourier transform of the resulting precession signal directly reflects the magnetic field distribution (broadened due to the muon lifetime). We have calculated theoretical field distributions within a two-component superconducting order parameter model appropriate for Sr_2RuO_4, and incorporated these results to calculate muon polarization functions as a function of the applied field, penetration depth λ, coherence length ξ and Fermi surface anisotropy ν (where $\nu = 0$ corresponds to a cylindrical Fermi surface, and $|\nu| = 1$ corresponds to a square Fermi surface). Although this model is strictly applicable only near H_{c2}, numerical calculations carried out over a wide range of fields yield only moderate changes from the approximations used here. In fitting the spectra to this theoretical model, we have used common values of $\kappa = 2.65$ and $|\nu| = 0.335$ (μSR is insensitive to the sign of ν which orients the vortex lattice with respect to the crystalline lattice), obtained from fitting several runs simultaneously. This value of $|\nu|$ is somewhat larger than expected on the basis of H_{c2} anisotropy and neutron diffraction measurements; nonlocal corrections not included in our theoretical model may account for some of this difference. The results of our analysis are shown in Fig. 77 for our $T_c(B = 0) =$ 1.48 K sample, where we plot $1/\lambda_{ab}^2$ vs. T for applied fields of 120 G (triangles) and 158 G (diamonds).

The temperature dependence of the superfluid density $n_s/m^* \propto 1/\lambda^2$ is fairly weak at low temperatures in Sr_2RuO_4, as is apparent from Fig. 77. Fitting to the temperature dependence of the superfluid density in weak coupling BCS theory gives the curves shown and provides an excellent fit to our data. Extrapolating these fits to low temperature, we obtain the zero temperature penetration depth $\lambda_{ab} = 1600$ Å for $B = 120$ G and $\lambda_{ab} = 1900$ Å for $B = 158$ G. Also shown in Fig. 77 is the low temperature linear temperature dependence of the superfluid density for the case of $YBa_2Cu_3O_{6.95}$ (which has line nodes) where we have scaled the axes to the T_c and $1/\lambda^2(T \to 0)$ values of Sr_2RuO_4. Clearly the behaviour of Sr_2RuO_4 is markedly different from that of the cuprates. While we are unable to exclude a small linear or T^2 term in $1/\lambda_{ab}^2$ at low temperatures, we can clearly exclude a large term such as exists in the cuprates. We stress that the excellence of the fit to the form of $1/\lambda_{ab}^2$

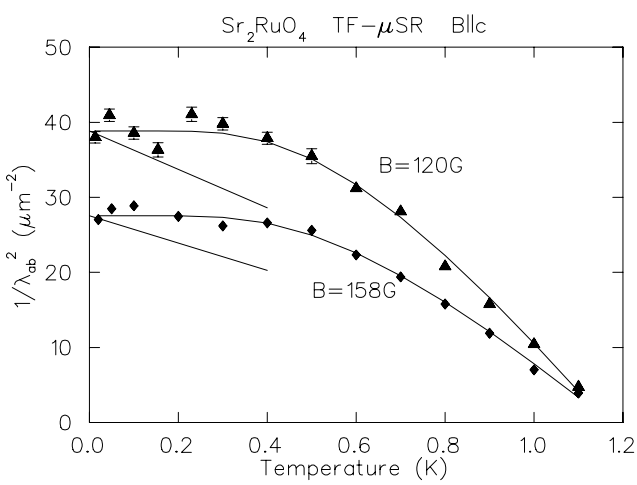

Fig. 77. Measured superfluid density ($1/\lambda^2 \propto n_s/m^*$) in Sr_2RuO_4 with the applied field $B \parallel \hat{c}$. Curves are fits to the temperature dependence of weak-coupled BCS theory, while lines follow reduced temperature dependence of $YBa_2Cu_3O_{6.97}$.

appropriate for weak coupling BCS theory does not mean that BCS is the correct theory for superconductivity in Sr_2RuO_4; rather, it indicates that the superconducting gap is fairly isotropic (and is likely characterized by weak coupling). As such, our measured results indicate that the gap in Sr_2RuO_4 is most likely nodeless, as expected for the previously identified E_u state.

Experiment 834
μSR study of transverse spin freezing in bond-frustrated magnets
(D.H. Ryan, McGill)

The random addition of antiferromagnetic (AF) exchange interactions to an otherwise ferromagnetic (FM) system leads to a loss of FM order through exchange frustration. In extreme cases, a spin glass (SG) is formed with random isotropic spin freezing and neither net magnetization nor long range order. At lower levels of frustration the system exhibits characteristics of both extremes as long-ranged FM order co-exists with SG order in the plane perpendicular to the FM order. On warming such a system from $T = 0$ K, the SG order first melts at T_{xy} followed by the loss of FM order at T_c. This picture has emerged from mean field calculations, numerical simulations and experimental measurements.

The aim of the current series of experiments is to investigate the magnetic behaviour in the region of T_{xy} in some partially frustrated alloys. Specifically, numerical simulations predict that although the freezing of transverse spin components does not represent a phase transition, it should be accompanied by significant, but non-critical, magnetic fluctuations.

Our first series of measurements confirmed that the expected signatures of transverse spin freezing could be observed using μSR (see 1999 Annual Report). However, there was a clear disagreement between the values for T_{xy} determined by μSR and those obtained earlier by applied field Mössbauer spectroscopy. The latter values were systematically lower, by as much as a factor of two in the most extreme case.

Measurements during our beam allocations in December, 1999 and May, 2000 were aimed at understanding this discrepancy. The first series focused on a–$Fe_{90-x}Ru_xZr_{10}$ for two reasons. (1) We can get cleanly into the fully frustrated state and so observe the FM→SG crossover. (2) We have been able to determine T_{xy} using zero-field Mössbauer spectroscopy in this system. The results, summarized as a phase diagram in Fig. 78, show much better agreement between the Mössbauer and μSR values for T_{xy}, indeed the Mössbauer values tend to lie slightly high in this system.

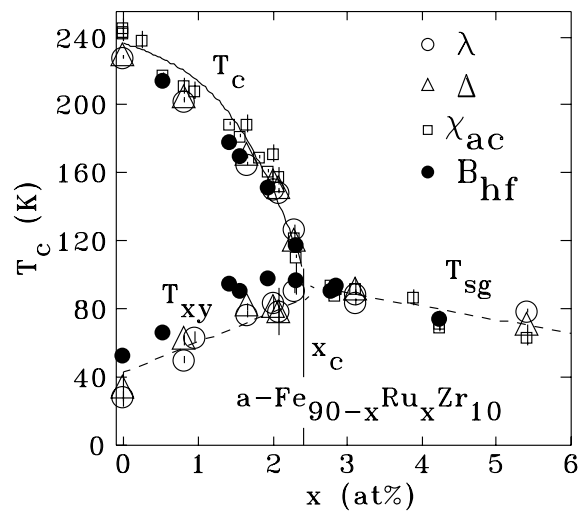

Fig. 78. Magnetic phase diagram for a–$Fe_{90-x}Ru_xZr_{10}$ showing T_c and T_{xy} deduced from μSR data. T_c's derived from χ_{ac} measurements on the same samples are also shown, as are T_c and T_{xy} values obtained using Mössbauer spectroscopy.

In May, we returned to the a–Fe_xZr_{100-x} system and concentrated around the $x = 93$ region in order to (i) confirm that the deviation from the applied field Mössbauer values for T_{xy} was a systematic effect, and (ii) determine the actual value for x_c, the composition at which the FM→SG crossover occurs. Previous estimates placed x_c around 94, while our initial μSR data from 1998 suggested that it lay below 93 (this seemingly minor issue matters because samples with $x > 93$ cannot be fabricated, and the value of $x_c = 94$ is an extrapolation). The results, summarized as a phase diagram in Fig. 79, confirmed that there is a clear systematic deviation between the applied field Mössbauer and zero-field μSR values for T_{xy}, suggesting that the ∼3 Tesla field used in the Mössbauer measurements greatly affects the value of T_{xy}. x_c was determined to lie at $x = 92.8$ in zero applied field.

Present status of Expt. 834

As we now know that the FM→SG crossover in a–Fe_xZr_{100-x} lies within the composition range that can be fabricated, we can study the full range of frustration effects in a binary rather than ternary alloy system, greatly simplifying sample quality control. We are now turning the discrepancy between the applied-field Mössbauer and zero-field μSR values for T_{xy} to our advantage. The observation offers a clean way in which to study the effects of an applied field on transverse spin freezing. Our final week of data-taking in May was devoted to following T_{xy} as a function of field in one sample. We were able to achieve a factor of four reduction in the available field of 5.5 Tesla, and confirmed that T_{xy} could indeed be observed in significant fields. This data set is currently being analyzed,

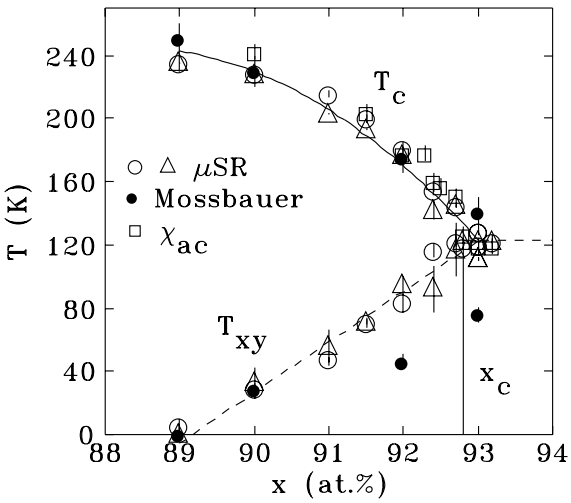

Fig. 79. Magnetic phase diagram for a–Fe_xZr_{100-x} showing T_c and T_{xy} deduced from μSR data. T_c's derived from χ_{ac} measurements on the same samples are also shown, as are T_c and T_{xy} values obtained on an independently prepared series of alloys measured using applied-field Mössbauer spectroscopy.

and we intend to follow this result with a systematic investigation across a wide range of compositions in the coming year.

Experiment 835
μSR studies on magnetic properties of layered superconductors HfNCl and ZrNCl
(T. Ito, Y.J. Uemura, Columbia)

Under Expt. 835 we have investigated a series of layered superconductors, HfNCl and ZrNCl. Organic molecules and alkali earth atoms may be intercalated between the layers in these materials, varying the interlayer spacing and doped charge respectively. Intercalated samples scale well in the universal correlation between T_c and the transverse field muon spin relaxation (TF-μSR) rate, σ, at the lowest temperature, which is observed in exotic superconductors including high-T_c cuprate superconductors.

We have measured the temperature dependence of the relaxation rate in TF-μSR at M20. The samples were aligned polycrystals mounted in a new In-sealed Kapton cell (prepared by Syd Krietzman *et al.*) to avoid decomposition by air. The spectra were analyzed using a cosine curve convoluted with Gaussian relaxation. As shown in Fig. 80, the temperature dependence of σ has a tendency to saturate at low temperatures and is quite similar to that of s-wave superconductivity, although it may be an artifact as is seen in polycrystalline high-T_c cuprate superconductors.

Correlation between T_c and $\sigma(T \to 0)$ is shown in Fig. 81. Samples co-intercalated with organic molecule THF show a simple correlation (a straight line), which

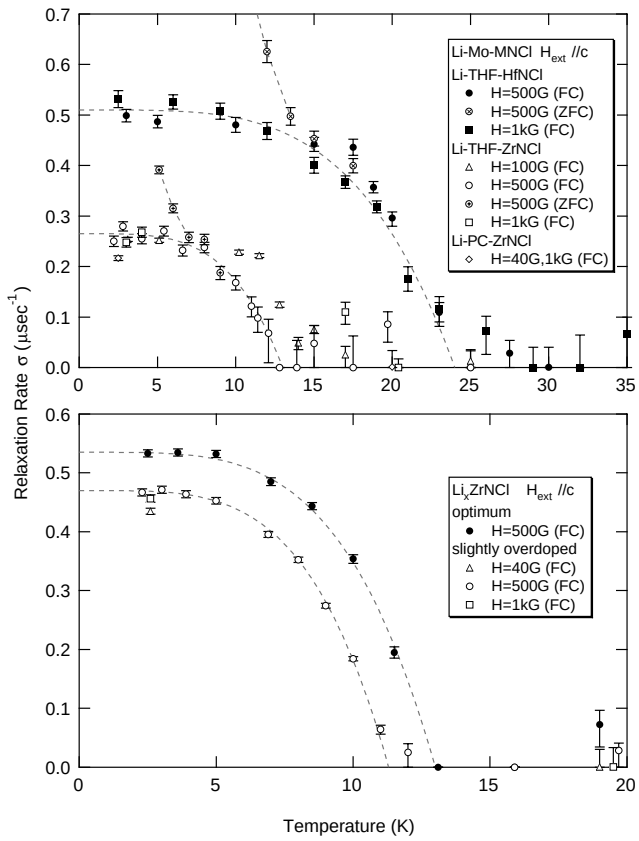

Fig. 80. TF-μSR relaxation rate vs. temperature in intercalated HfNCl and ZrNCl.

is observed in exotic superconductors such as high-T_c cuprate superconductors. All of these compounds have almost the same c-axis lattice constant (13.3 Å). On the other hand, the samples without organic molecules,

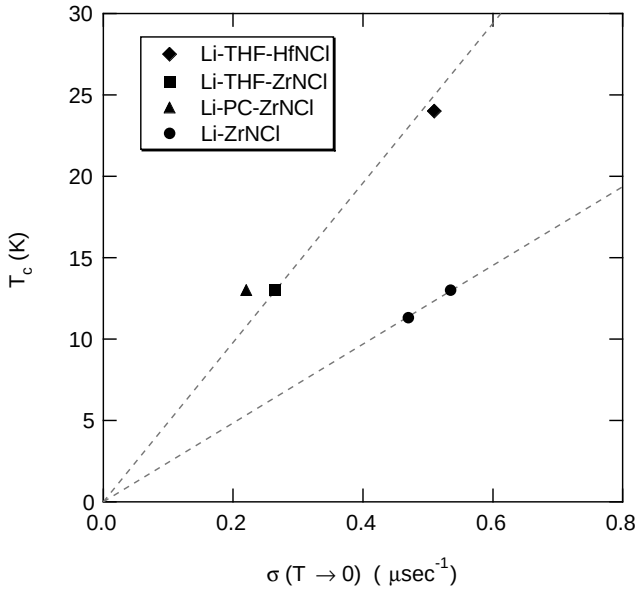

Fig. 81. The $T \to 0$ K relaxation rate vs. T_c for intercalated HfNCl and ZrNCl.

whose c-axis lattice constant is 9.4 Å, have a different slope in Fig. 81, which is closer to that expected for conventional BCS superconductors.

Further experiments will be performed using samples with (i) larger interlayer spacing and (ii) a wide range of carrier concentrations.

Experiment 842
Muonium-substituted free radicals in sub- and supercritical water

(P.W. Percival, SFU)

Experiment 842 was originally conceived to study free radicals formed in reactions of muonium with organic compounds dissolved in water at high temperatures and pressures. However, given the remarkable results of Expt. 713, reported in last year's Annual Report, the focus of this year's efforts has remained on studies of muonium reaction kinetics rather than free radical products. On a pragmatic note, the delay in free radical studies provides a better match with the timing of necessary apparatus development and funding.

The kinetics studies entail measurements of muonium decay rates in dilute aqueous solutions of the appropriate reactants, as a function of both temperature and pressure. During the past year we completed comprehensive studies of several reactions: Mu + hydroquinone, Mu + OH^-, Mu + I^-, and Mu + benzene. Preliminary results for the first three reactions were shown in the 1999 Annual Report; some data for the reaction with benzene are shown in Figs. 82 and 83. New in 2000 was a study of the reaction of Mu with alcohols (Fig. 84).

The motivation for these studies is to determine muonium rate constants under the extreme conditions found in supercritical water reactors, used for the destruction of hazardous waste, and in the cooling water cycles of pressurized water nuclear reactors. Since muonium behaves chemically as a light isotope of hydrogen, it can be used to study H atom chemistry and the properties of free radicals which incorporate H (almost all organic free radicals).

For many reactions there is a significant "kinetic isotope effect", i.e. the Mu and H rate constants are not equal. Nevertheless, a study of the temperature and pressure dependence of the Mu rate constant can provide novel data of general applicability to reactions in water under extreme conditions. Thus, our demonstration of a maximum in the rate constant as a function of temperature has obvious relevance to the efficiency of supercritical water reactors used for waste destruction.

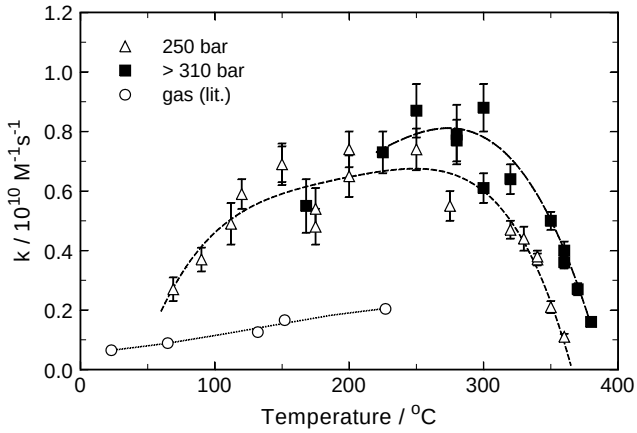

Fig. 82. Rate constants for Mu + benzene in water at two pressures, compared with literature data for gas phase measurements [Roduner, Fleming *et al.*, Ber. Bunsenges. Phys. Chem. **94**, 1224 (1990)].

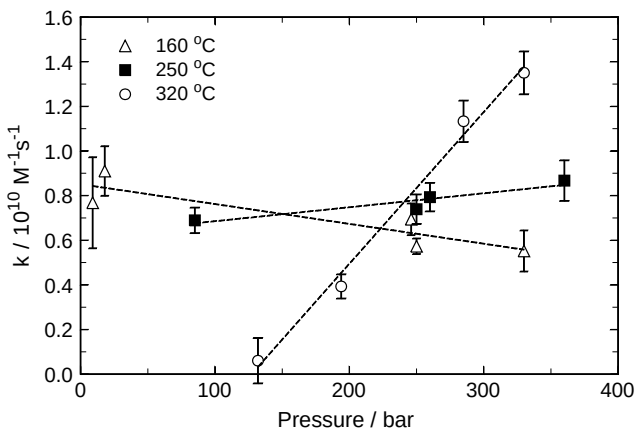

Fig. 83. Pressure dependence of rate constants for Mu + benzene in water at selected temperatures.

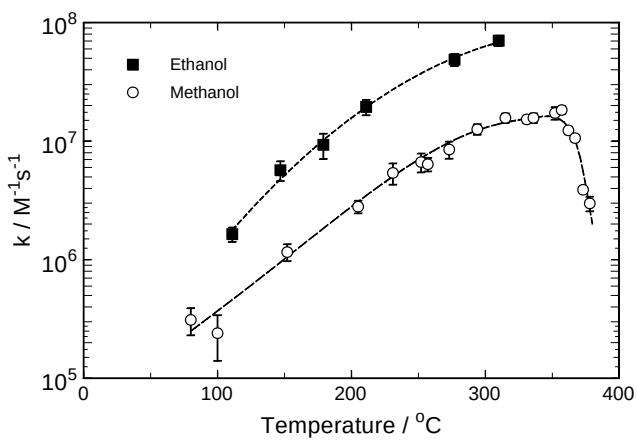

Fig. 84. Rate constants for Mu + alcohols in water at 230 bar.

Another example concerns the chemistry of radiolysis transients (hydrogen atoms, hydroxyl radicals, hydrated electrons) in the cooling water cycle of pressurized water nuclear reactors. The nuclear industry uses

a model for high temperature water radiolysis based on extrapolation of lower temperature data. The available data on the reactions of hydrogen atoms is very sparse and stops well short of the maximum temperature attained in our experiments. As a consequence, the extrapolated data for H atom kinetics shows curvature, but no maximum with temperature as found for Mu.

We have found a rate constant maximum for a wide diversity of reaction types:

addition:

$$\mathrm{Mu} + \mathrm{C_6H_6} \rightarrow \mathrm{C_6H_6Mu}$$

abstraction:

$$\mathrm{Mu} + \mathrm{CH_3OH} \rightarrow \mathrm{MuH} + \mathrm{CH_2OH}$$

muon transfer:

$$\mathrm{Mu} + \mathrm{OH^-} \rightarrow \mathrm{MuOH} + \mathrm{e^-_{aq}}$$

spin exchange:

$$\mathrm{Mu}(\uparrow) + \mathrm{Mn^{2+}}(\downarrow) \rightarrow \mathrm{Mu}(\downarrow) + \mathrm{Mn^{2+}}(\uparrow)\ .$$

This suggests that the maximum is due to some general phenomenon, such as the change in structure of the solvent as the conditions change.

A good clue to the explanation is given by the difference between the high pressure condensed phase data and the low pressure gas phase results (see Fig. 82). Such a situation is often ascribed to the "cage effect": reactants in liquids are constrained by the surrounding solvent molecules so that an encounter between reaction partners results in multiple collisions, increasing the probability of reaction over the single collision encounters that occur in gases. This effect should be important for diffusion-controlled reactions in liquid water, where hydrogen-bonded water molecules associate to form transient structures around solutes. However, the density of water falls markedly as the temperature approaches the critical point, and structural change is inevitable.

Thus the temperature dependence displayed in Fig. 82 can be qualitatively described in terms of the transition from *activation* control (where the chemical reaction is the rate-determining process) to partial *diffusion* control (chemical reaction is as fast as the inverse lifetime of reactant encounter pairs) to *collision* control. The different regimes appear to be characterized by markedly different pressure dependence (Fig. 83). In the case of a slow reaction, such as H abstraction (Fig. 84), the rate constant increases with temperature but does not reach the diffusion limit before the onset of the collision-controlled regime.

Quantitative analysis and interpretation of these data is ongoing, and, together with earlier results from Expts. 713 and 842, will comprise the Ph.D. thesis of Khashayar Ghandi, who won the 1999/2000 Westcott Fellowship for graduate research at TRIUMF.

Experiment 846
Complex order parameter symmetry in $YBa_2Cu_3O_{7-\delta}$ at low T and high magnetic field
(J.H. Brewer, TRIUMF/UBC; J.E. Sonier, SFU)

In 2000 we carried out a zero-field (ZF) μSR study of the superconducting $YBa_2Cu_3O_{6+x}$ system. The aim was to gain new insight into the role of the pseudogap (PG) phase in high-temperature superconductivity by exploiting the uniqueness of the muon as a local probe of magnetic and electronic properties. At issue is whether or not the PG is a *true* phase transition and whether or not it competes with superconductivity.

We investigated high purity $x = 0.67$ and $x = 0.95$ single crystals (with superconducting transition temperatures $T_c = 93.2(3)$ K and 67.9(1.2) K, respectively)

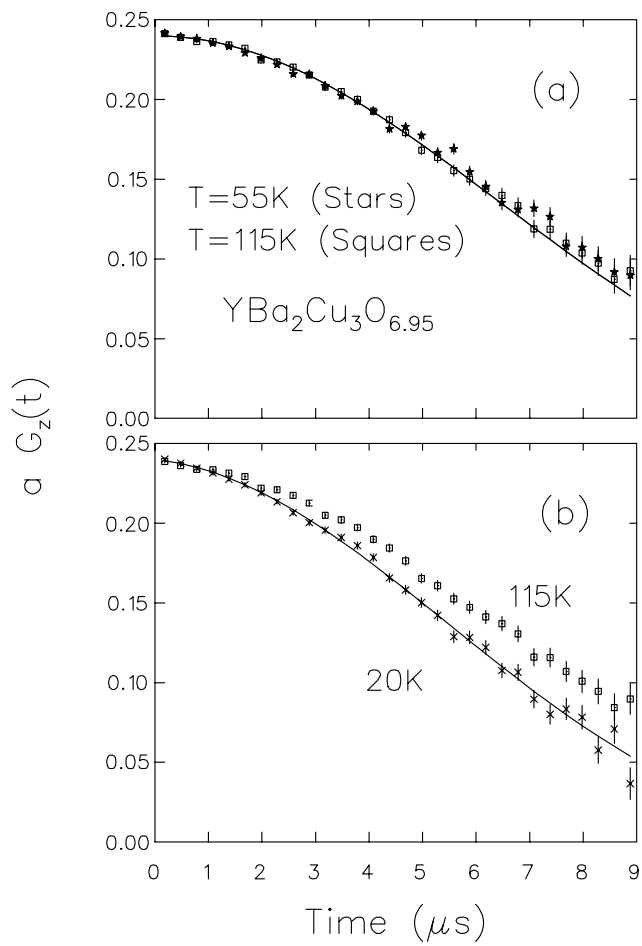

Fig. 85. The time evolution of the muon spin polarization in zero external field for $YBa_2Cu_3O_{6.95}$ crystals measured with the initial polarization $P_\mu(0)$ perpendicular to the c-axis. (a) Measurements taken above and below T_c at 115 K and 55 K, respectively. The solid curve is a fit to a Kubo-Toyabe (KT) function describing the depolarization of the muon spin by the nuclear dipoles. (b) Measurements taken above and below T_c at 115 K and 20 K, respectively. The solid curve through the 20 K data is a fit to the KT function multiplied by an exponential function $\exp(-\lambda t)$.

grown at the University of British Columbia. Our study revealed the presence of small spontaneous magnetic fields of electronic origin that appear to be related to the PG transition. Figure 85 shows the measured time evolution of the muon spin polarization in the $x = 0.95$ crystals for the case in which the initial spin polarization $P_\mu(0)$ is perpendicular to the c-axis. The relaxation observed in Fig. 85a is that due to the randomly oriented static magnetic fields of the nuclear dipoles. However, on cooling below 47 K there is a marked increase in the ZF relaxation rate (see Fig. 85b), signifying the occurrence of a small additional magnetic field at temperatures well below T_c. The additional signal relaxation was best described by an exponential function $\exp(-\lambda t)$ and was found to vanish in an applied magnetic field of 0.5 kOe. This suggests that the small magnetism originates from dilute moments of some kind which are static or fluctuating very slowly. The results of ZF measurements in the $x = 0.95$ sample for two different orientations of the initial muon spin polarization $P_\mu(0)$ are summarized in Fig. 86.

In the $x = 0.67$ sample the onset of small spontaneous magnetic fields occurred well above T_c at $\approx$170 K (see Fig. 87). This temperature is near the PG transition temperature T^* determined by other methods. Thus it appears that the small magnetic fields are intimately related to the PG phase, and that the PG coexists with superconductivity. Our findings are difficult to reconcile with current theories predicting the onset of a dense array of circulating currents at T^*.

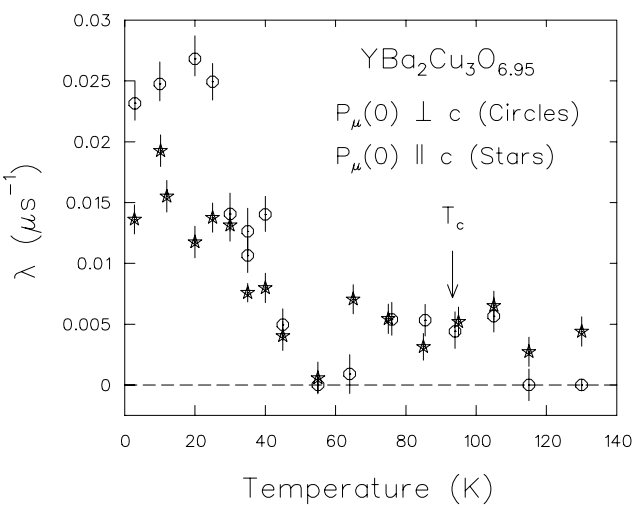

Fig. 86. The temperature dependence of the ZF exponential relaxation rate λ in $YBa_2Cu_3O_{6.95}$. Measurements were taken with the initial muon spin polarization $P_\mu(0)$ perpendicular (circles) and parallel (stars) to the c-axis of the crystals. The increase below $T \approx 47$ K signifies the onset of a small spontaneous magnetic field.

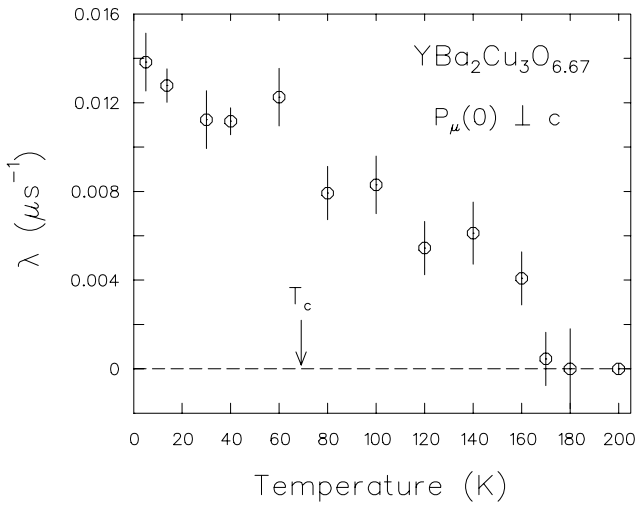

Fig. 87. The temperature dependence of the ZF exponential relaxation rate λ in $YBa_2Cu_3O_{6.67}$. Measurements were taken with the initial muon spin polarization $P_\mu(0)$ perpendicular to the c-axis of the crystals. The increase below $T \approx 170$ K signifies the onset of a small spontaneous magnetic field.

Experiment 847
Electron-doped high-T_c superconductors
(J.E. Sonier, SFU)

The identity of the pairing symmetry in the *electron-doped* high-T_c superconductors is an unsettled issue. Many of the early experiments suggested an s-wave pairing symmetry, differing from the established d-wave symmetry in *hole-doped* high-T_c superconductors. Experiment 847 was proposed to address this issue by performing *bulk* measurements of the magnetic penetration depth λ. Similar measurements in $YBa_2Cu_3O_{7-\delta}$ [Sonier *et al.*, Phys. Rev. Lett. **74**, 722 (1994); *ibid.* **79**, 2875 (1997)] contributed to the identification of the d-wave symmetry in the hole-doped materials.

In June we used the newly developed MULTI spectrometer to carry out μSR measurements on tiny crystals of $Pr_{2-x}Ce_xCuO_{4+\delta}$ grown at the University of Maryland. Because the muon counter of the MULTI spectrometer lies within the cryostat directly in front of the sample, the beam momentum could be reduced without increasing the background signal from muons stopping upstream in the cryostat window. This made it possible to measure crystals weighing as little as 3 mg. Figure 88 shows the fast Fourier transform of the muon spin precession signal in a small single crystal of $Pr_{2-x}Ce_xCuO_{4+\delta}$ at H = 200 Oe. This is the first time that the internal magnetic field distribution has been observed in this material. The ability to measure such small samples demonstrates the remarkable recent advancements in μSR spectrometer design.

Figure 89 shows the temperature dependence of the muon depolarization rate σ in $Pr_{2-x}Ce_xCuO_{4+\delta}$. It is

clear that there is a sizeable moment associated with the Pr^{3+} ion even at the lower temperatures, as evidenced by the increase of σ with decreasing temperature in the normal state. This means that crystal electric field (CEF) excitations are relevant over the temperature range of interest, since the CEF ground state of the Pr^{3+} ion is nonmagnetic. This information is important for the interpretation of experimental data obtained with other techniques. The onset of superconductivity is visible as a kink in the plot of Fig. 90, where σ is enhanced due to the broad internal field distribution associated with the formation of a vortex lattice.

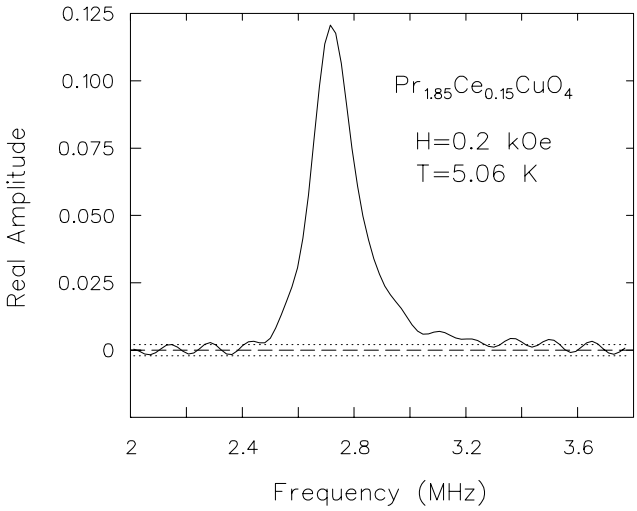

Fig. 88. The fast Fourier transform of the muon spin precession signal in $Pr_{2-x}Ce_xCuO_{4+\delta}$ after field cooling to $T = 5.06$ K in a magnetic field H = 200 Oe.

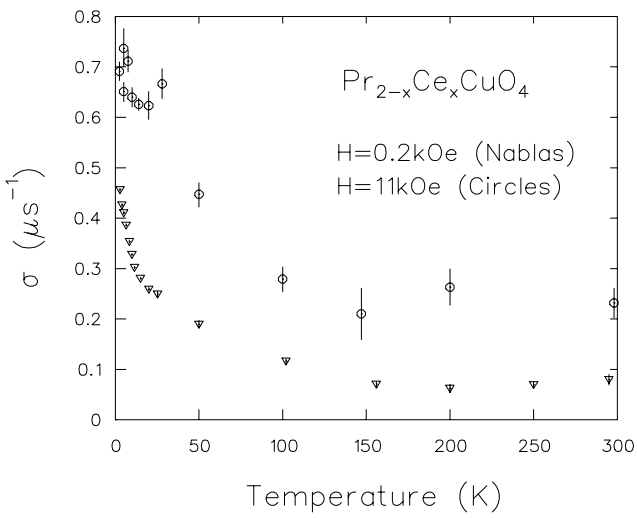

Fig. 89. Temperature dependence of the muon Gaussian depolarization rate σ in $Pr_{2-x}Ce_xCuO_{4+\delta}$ at H = 0.2 kOe and H = 11 kOe. The 0.2 kOe data were collected using the MULTI spectrometer, whereas the 11 kOe data were taken using the standard low-background insert.

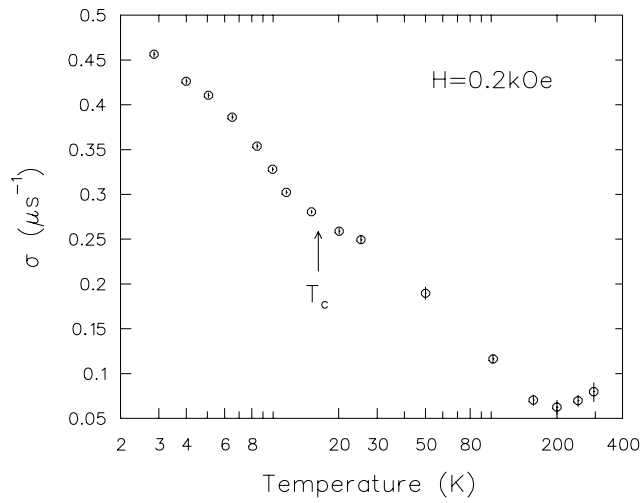

Fig. 90. Temperature dependence of the muon Gaussian depolarization rate σ.

The paramagnetism associated with the Pr^{3+} ions broadens the μSR line shape measured in the vortex state below the superconducting transition temperature T_c. In principle, this additional contribution to the linewidth can be separated from the field distribution associated with the vortex structure.

Experiment 849
Static magnetism in stage-4 $La_2CuO_{4.12}$ and $La_{1.88}Sr_{0.12}CuO_4$
(Y.J. Uemura, Columbia; K.M. Kojima, Tokyo)

The purpose of our experiment was to study superconducting samples of $La_2CuO_{4.12}$ and $La_{1.88}Sr_{0.12}CuO_4$. Single crystals were mounted in a He gas flow cryostat, which can attain temperatures down to 2 K. μSR measurements were performed for two different orientations of the crystal: with the muon beam (and muon polarization) parallel and perpendicular to the c-axis.

At high temperatures the spectra show a slow relaxation due to nuclear dipolar fields. Below 42 K for $La_2CuO_{4.12}$ and 20 K for $La_{1.88}Sr_{0.12}CuO_4$ the spectra exhibit a Bessel-like oscillation, characteristic of incommensurate spin-density-wave (SDW) ordering.

We found that the oscillation amplitude is significantly less than expected for the case where all incident muons reside at sites with spontaneous magnetic fields. This feature can be understood if static spin freezing occurs only in a part of the sample volume. Here we analyze our data assuming this situation, with V_M denoting the volume fraction with static spin freezing.

In order to find V_M, measurements are required for two different orientations of the crystals. The procedure and numerical values were published in Physica B [Savici *et al.*, Physica **B289-290**, 338 (2000)]. In the upper part of Fig. 91 we show the magnetic volume fraction for $La_2CuO_{4.12}$ and $La_{1.88}Sr_{0.12}CuO_4$ and we

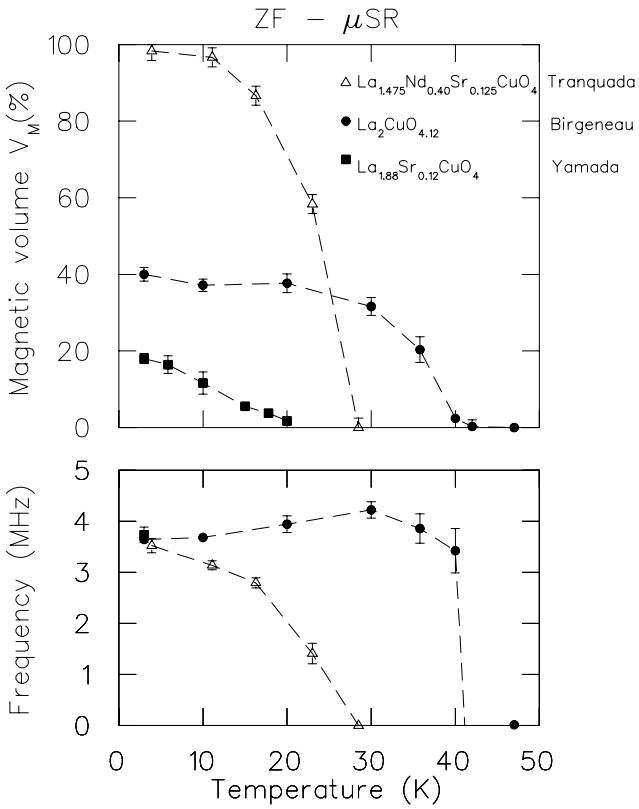

Fig. 91. Magnetic site fraction with static magnetic ordering and frequency of the precessing signal for $La_2CuO_{4.12}$, $La_{1.88}Sr_{0.12}CuO_4$ and $La_{1.475}Nd_{0.4}Sr_{0.125}CuO_4$.

compare them to $La_{1.475}Nd_{0.4}Sr_{0.125}CuO_4$ for which we have data from a previous measurement.

The lower part of Fig. 91 shows that the frequency of the oscillating signal for $La_2CuO_{4.12}$ increases very sharply below T_N and rapidly attains a constant value of 3.6 MHz. For $La_{1.88}Sr_{0.12}CuO_4$ we were able to determine this frequency only at very low temperature. This frequency is very close to that observed by μSR in $La_{1.475}Nd_{0.4}Sr_{0.125}CuO_4$ and many other "1/8" systems, indicating that the local spin structure of the frozen Cu moments is identical among these three specimens. The observed frequency corresponds to a modulated static Cu moment with a maximum amplitude of about 0.3–0.4 μ_B, as scaled from the 5 MHz μSR frequency in undoped La_2CuO_4, which has 0.5–0.6 μ_B per Cu.

Experiment 852
Magnetic phases in geometrically frustrated rare earth pyrochlores

(S. Dunsiger, R. Kiefl, UBC; J. Gardner, NRC)

In systems where magnetic ions occupy the vertices of edge or corner sharing triangular units, there is no spin configuration which simultaneously satifies all the magnetic couplings if all these interactions are *antiferromagnetic*. Stacked triangular, kagomé, fcc, and pyrochlore lattices are all examples of this *geometric* frustration. The purpose of Expt. 852 is to apply μSR to further our understanding of the effect of this frustration on the ground state and low lying magnetic excitations in the pyrochlores $A_2B_2O_7$, where magnetic ions form a network of corner sharing tetrahedra. Unlike many other systems having geometric frustration, pyrochlores are noted for their high degree of chemical order, which is important for isolating effects due to geometric frustration. Also, it is now possible to grow high quality single crystals of rare earth titanates such as $Tb_2Ti_2O_7$, $Gd_2Ti_2O_7$ and $Ho_2Ti_2O_7$.

A system of Heisenberg spins interacting via nearest-neighbour antiferromagnetic couplings on the pyrochlore lattice displays a classical ground state with macroscopic degeneracy, since the lowest energy spin configuration requires only that $\Sigma_{i=1}^4 \mathbf{S}_i = 0$ for each tetrahedron. This feature led Villain to argue that these systems remain in a *cooperative paramagnetic* state with only short range spin-spin correlations for all T > 0 [Villain, Z. Physik **B33**, 31 (1979)] and this has been confirmed by Monte Carlo simulations [Reimers, Phys. Rev. **B45**, 7287 (1992)]. However, additional factors such as magnetic anisotropy, further nearest neighbour exchange and fluctuations [Bramwell *et al.*, J. Appl. Phys. **75**, 5523 (1994)] can lift the degeneracy and lead to Néel order involving complicated canted structures, as observed in $Nd_2Mo_2O_7$ [Greedan *et al.*, Phys. Rev. **B43**, 5682 (1991)] and possibly other more exotic ground states.

Oxide pyrochlores where the B site is occupied by a magnetic ion (typically a transition metal) often exhibit a type of ordering, with freezing temperatures in the range of 20–100 K. Muon spin relaxation has been important in identifying and characterizing the spin glass states in $Y_2Mo_2O_7$ and $Tb_2Mo_2O_7$ [Dunsiger *et al.*, Phys. Rev. **B54**, 9019 (1996)]. However, if magnetic ions are present on both the A and B sites it is more difficult to isolate the contributions from each species. The rare-earth (RE) titanate pyrochlores are interesting since the Ti^{4+} ion is nonmagnetic and thus there is only one magnetic species.

$Ho_2Ti_2O_7$: a spin ice

Water ice is made up of oxygen atoms which form a hexagonal lattice (Wurtzite structure). Of the 4 hydrogen atoms arranged tetrahedrally around each oxygen atom, two form strong covalent O−H bonds and are close to it to form a water molecule; the remaining two are hydrogen bonded and further removed. In a crystal of 2N bonds there are 2^{2N} possible ways of arranging the protons, not all of which satisfy these Bernal-Fowler ice rules [Pauling, *The Nature of the Chemical Bond* (Cornell Univ. Press, 1960) p.465]. Out of 2^4 =

16 ways of arranging the bonds around a single oxygen, only 6 satisfy this condition. The total number of allowed configurations is therefore of the order of $(6/16)^{\mathrm{N}}2^{2\mathrm{N}} = (3/2)^{\mathrm{N}}$. Experimentally, the associated residual entropy is found to be close to the theoretical value $S_0 = \mathrm{N}k_B \ln(3/2)$ at zero temperature. Although the H disorder can be represented as configurational entropy, there is no clear violation of the third law of thermodynamics. This is because energy barriers of the order of 1 eV would have to be surmounted to establish long range order in hydrogen ion position. As a result, relaxation through tunnelling into a lower entropy state is an extremely slow process below ice's freezing temperature and the system is therefore not in thermal equilibrium.

The hydrogen ion bonds between atoms form electric dipoles, so they can conveniently be represented by arrows placed on the bonds pointing towards the end occupied by the ion. The ice rule is then equivalent to saying that at each site there are two arrows in and two out, as shown in Fig. 92. Spin orientation thus plays a similar role to that of hydrogen position in ice and magnetic analogues of water ice, so called "spin ice", are currently of extreme interest [Ramirez *et al.*, Nature **399**, 333 (1999); Harris, Nature **399**, 311 (1999)]. Moessner [Phys. Rev. **B57**, R5587 (1998)] shows that a strongly anisotropic classical Heisenberg model on the pyrochlore lattice can be mapped onto an Ising pseudospin model with an exchange constant opposite in sign. In the case of strong anisotropy ($|\mathcal{J}/D| \ll 1$) the anisotropy term dominates, constraining the spins to lie along the $\langle 111 \rangle$ axes. The exchange term defines the direction in which they point, such that the enclosing angle between any pair may only take on values of 70.5° or 109.5°. Thus, counterintuitively, a system of spins situated on the vertices of corner sharing tetrahedra where the interactions are *ferromagnetic* may also be geometrically frustrated, provided the spins are constrained by anisotropy to point along the $\langle 111 \rangle$ axes.

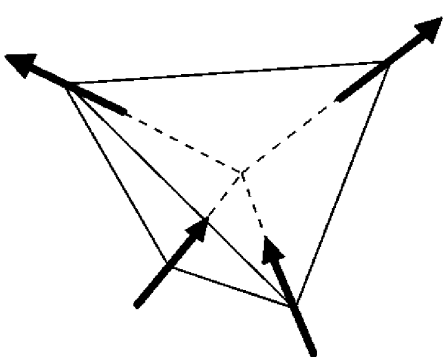

Fig. 92. Ground state configuration of spins on a single tetrahedron given ferromagnetic interactions and strong easy axis anisotropy along the dashed lines.

Experimentally, the magnetic ions in a number of pyrochlores have recently been found to be subject to significant single ion anisotropies, whose local easy axis is along the $\langle 111 \rangle$ directions and which are thus candidates for spin ice behaviour. To date, the most extensively studied spin ice material is $Ho_2Ti_2O_7$ [Harris *op. cit.*; Harris *et al.*, J. Magn. Magn. Mater. **177-181**, 757 (1998)]. The Ho^{3+} ion is Ising-like due to crystal field splittings which result in a ground state doublet with $J_z = \pm 8$ and the next excited state ~250 K higher [Siddharthan *et al.*, Phys. Rev. Lett. **83**, 854 (1999)]. This suggests that at low temperatures $Ho_2Ti_2O_7$ is well described as a quasi spin 1/2 Ising system. Neutron scattering measurements indicate that no long range order develops down to temperatures of at least 0.35 K in zero magnetic field, but instead, short range ferromagnetic correlations are observed [Harris *et al.*, J. Magn. Magn. Mater. *op. cit.*]. The idea which seems to be emerging is that there is no phase transition to a spin glass state, for example, but rather a continuous slowing down of spin fluctuations as the temperature is reduced, due to the development of energy barriers. A number of ordered phases have also been observed on application of a magnetic field, as well as history dependent behaviour. Monte Carlo simulations by Harris *et al.* [Phys. Rev. Lett. **81**, 4496 (1998)] show that the degree of degeneracy breaking depends on the direction of the applied field relative to the crystal axes and this has been confirmed by dc magnetization measurements (see Fig. 93).

Monte Carlo simulations have been able to describe the magnetic susceptibility and diffuse magnetic neutron scattering results well, but the nature of the spin

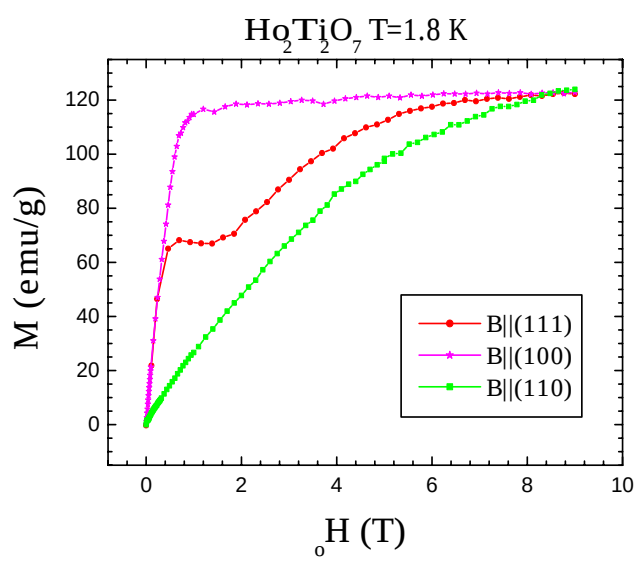

Fig. 93. DC magnetization as a function of applied magnetic field in $Ho_2Ti_2O_7$ [Cornelius, unpublished].

dynamics has only been very briefly studied in low field [Harris *et al.*, J. Magn. Magn. Mater. *op. cit.*]. In June and October we carried out a series of $1/T_1$ measurements on the $\langle 100 \rangle$ and $\langle 110 \rangle$ orientations of $Ho_2Ti_2O_7$ in the dilution refrigerator on M15. In a low longitudinal field (LF) of 0.003 T the μ^+ spin depolarized too quickly to be observed. This is attributed to rapid Ho^{3+} spin fluctuations in the paramagnetic regime.

$Ho_2Ti_2O_7$ ($\boldsymbol{H} \parallel \langle 100 \rangle$)

Typical spectra at a higher field of 2 T are shown in Fig. 94. In this case a component of *all* the Ho spins lies along the applied field direction, since they point along the $\langle 111 \rangle$ directions. As shown in Fig. 95, the

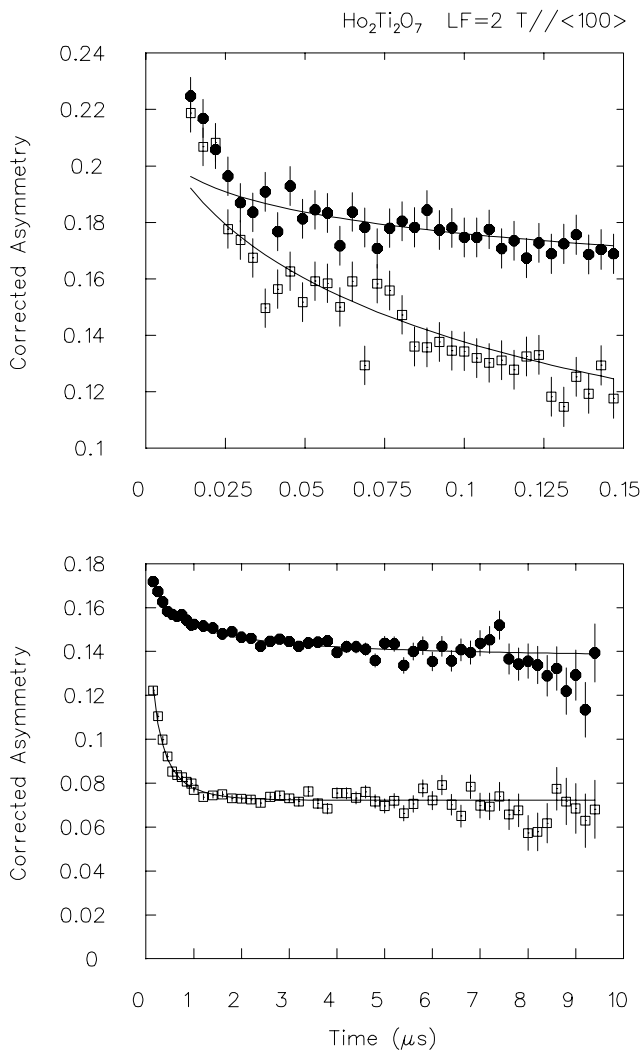

Fig. 94. Typical spectra in $Ho_2Ti_2O_7$ in a longitudinal field of 2 T applied along the $\langle 100 \rangle$ direction.

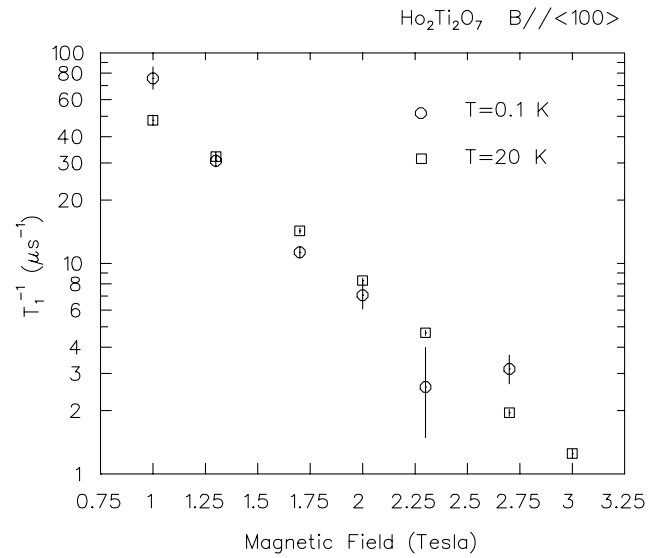

Fig. 95. Relaxation rate of muon spin polarization in $Ho_2Ti_2O_7$ as a function of applied magnetic field (along the $\langle 100 \rangle$ direction).

relaxation rate $1/T_1$ decreases with increasing field at 20 K. The decrease is likely because the spin dynamics are being altered as the electronic Zeeman splitting first becomes comparable with and then exceeds the exchange coupling $\mathcal{J}$. Extrapolating back to zero field, $1/T_1$ is in excess of 100 μs^{-1}. In low longitudinal field experiments in the "motionally narrowed" limit of rapid spin fluctuations

$$1/T_1 = \frac{2\Delta^2}{\nu},$$

where $\Delta^2/\gamma_\mu^2 = \langle B_i^2 \rangle$ is the second moment of the internal magnetic field B_i ($i = x, y, z$), ν is the mean fluctuation rate for fluctuations in B_i, and γ_μ is the muon gyromagnetic ratio. The spin fluctuation rate can thus be roughly estimated at ~10 GHz, assuming $\Delta/\gamma_\mu = 0.70(6)$ T from studies* of the isostructural compound $Tb_2Mo_2O_7$ [Dunsiger *et al., op. cit.*], since the free Ho^{3+} and Tb^{3+} ions have comparable magnetic moments of 10.4 and 9.5 μ_B respectively. This is below the timescales accessible by neutron scattering; hence μSR is uniquely sensitive to the spin dynamics in these spin ice materials, which have not previously been studied.

The results of temperature scans in longitudinal fields of 2 and 3 T are summarized in Figs. 96 and 97. Above 5 K the data are well described by a stretched exponential function. The muon spin relaxation rate decreases with temperature as $\mu_B H/k_B T$ grows and the sample becomes increasingly magnetized. However,

* In $Tb_2Mo_2O_7$ one can measure the magnitude of H_i directly since spin freezing is observed.

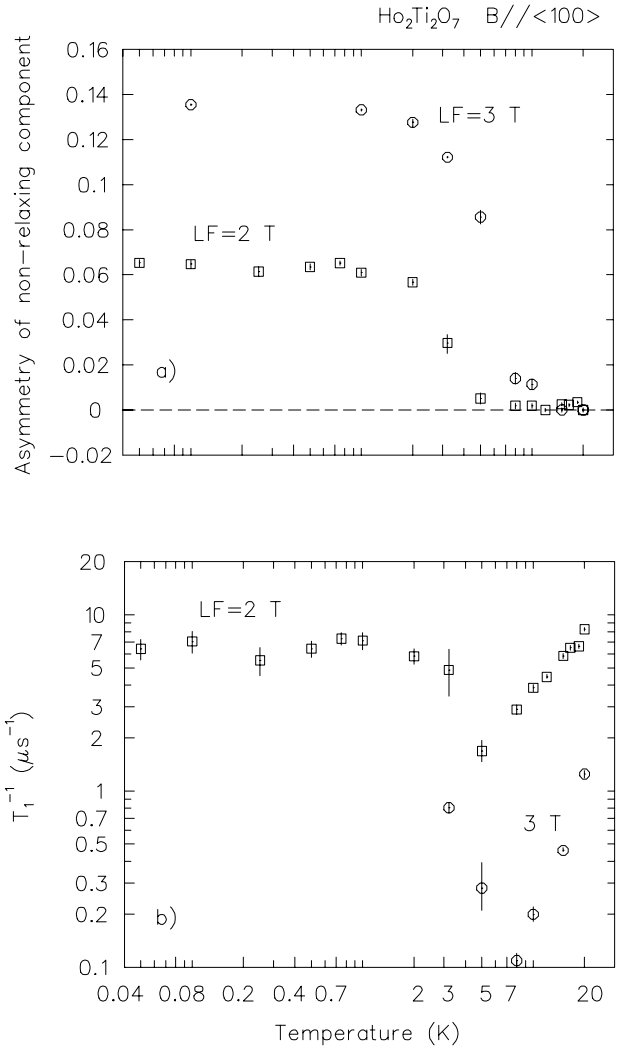

Fig. 96. a) Asymmetry of non-relaxing component and b) relaxation rate of muon spin polarization in $Ho_2Ti_2O_7$ as a function of temperature.

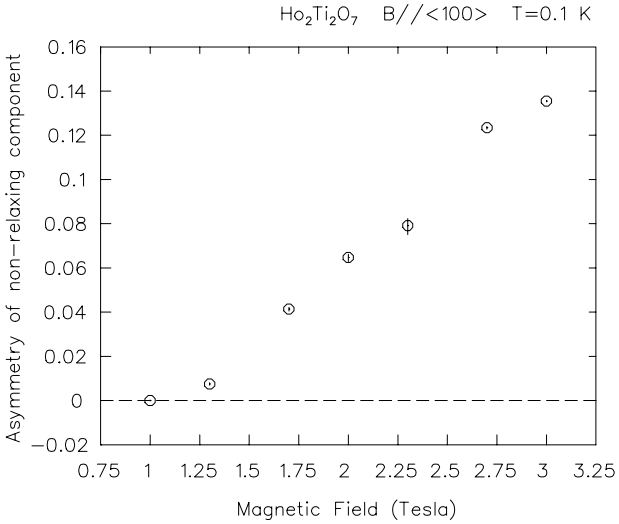

Fig. 97. Asymmetry of non-relaxing component as a function of magnetic field in $Ho_2Ti_2O_7$ at 0.1 K.

below 5 K a non-relaxing component develops at the expense of the amplitude of the relaxing component, such that almost the full amplitude of ∼0.16 is non-relaxing at 3 T. The decoupling curve shown in Fig. 97 suggests that a static component of the order of 1 T develops. The residual relaxing component is thought to be *dynamic* in nature. If the muon spin depolarization were due to a static internal field Δ of the order of 1 T, it would take place on a time scale of $\Delta^{-1} \approx 1$ ns, too fast to be observed. It is, however, difficult to understand such two component behaviour in a system of dense spins on crystallographically equivalent sites.

To better understand the non-relaxing component, a few preliminary transverse field (TF) measurements have been made very recently. The Curie-like dependence of the muon spin precession frequency above 100 K is anticipated in the paramagnetic state (see Fig. 98). However, the signal oscillating at ∼160 MHz shown in Fig. 99 is indicative of internal magnetic fields of roughly 1 T, which are static at least on the timescale of 10 ns. The size of the static internal field is consistent with the LF scans. However, the signal persists at 5 K, in contrast with the development of the non-relaxing component in the LF measurements. This may be due to hysteresis effects.

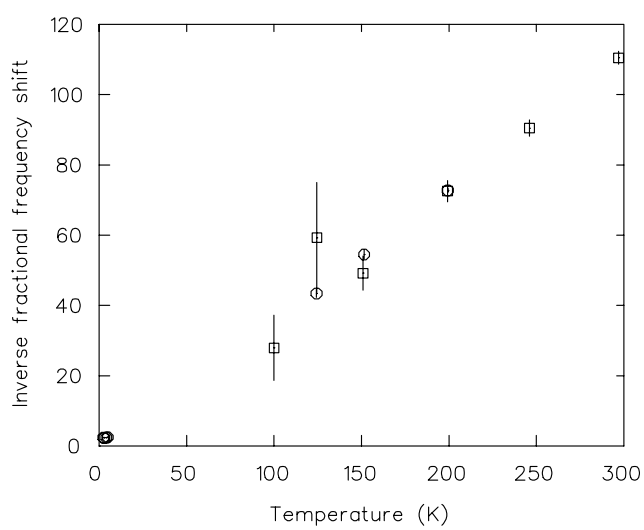

Fig. 98. Inverse paramagnetic frequency shift of the muon spin precession in $Ho_2Ti_2O_7$ in 0.099 and 2 T ($H \parallel \langle 100 \rangle$).

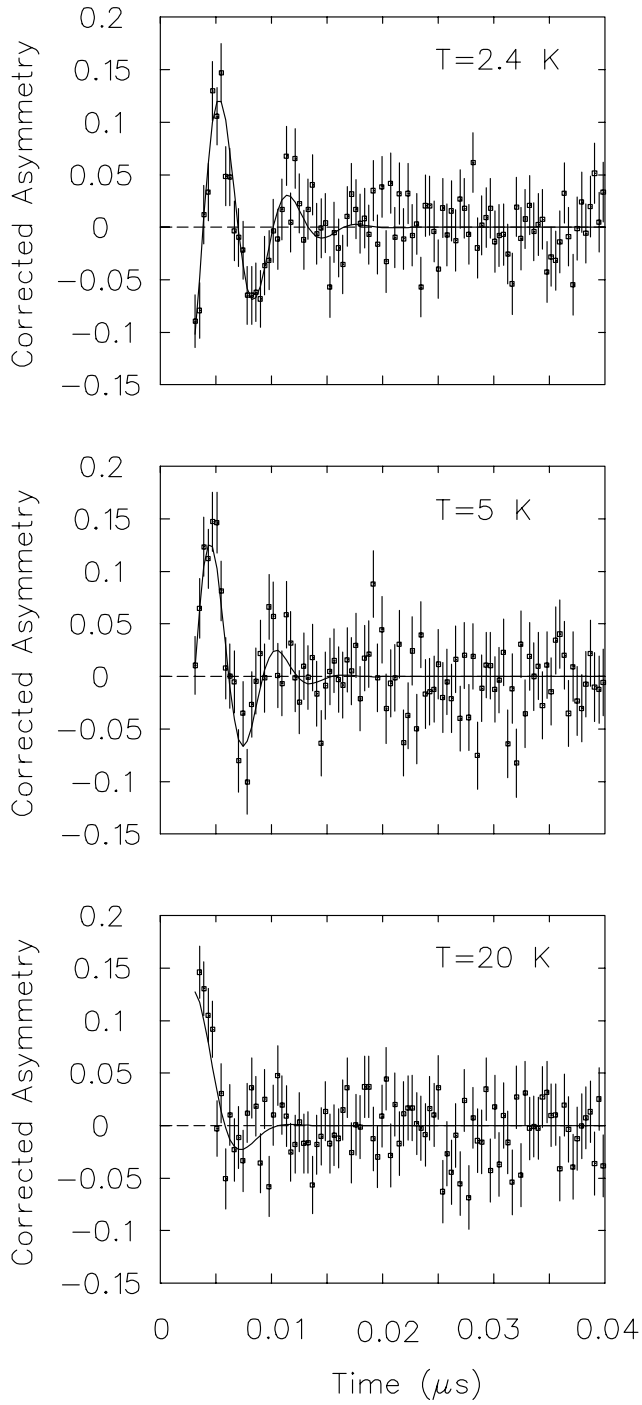

Fig. 99. Typical spectra in $Ho_2Ti_2O_7$ in a TF = 2 T ($H \parallel \langle 100 \rangle$).

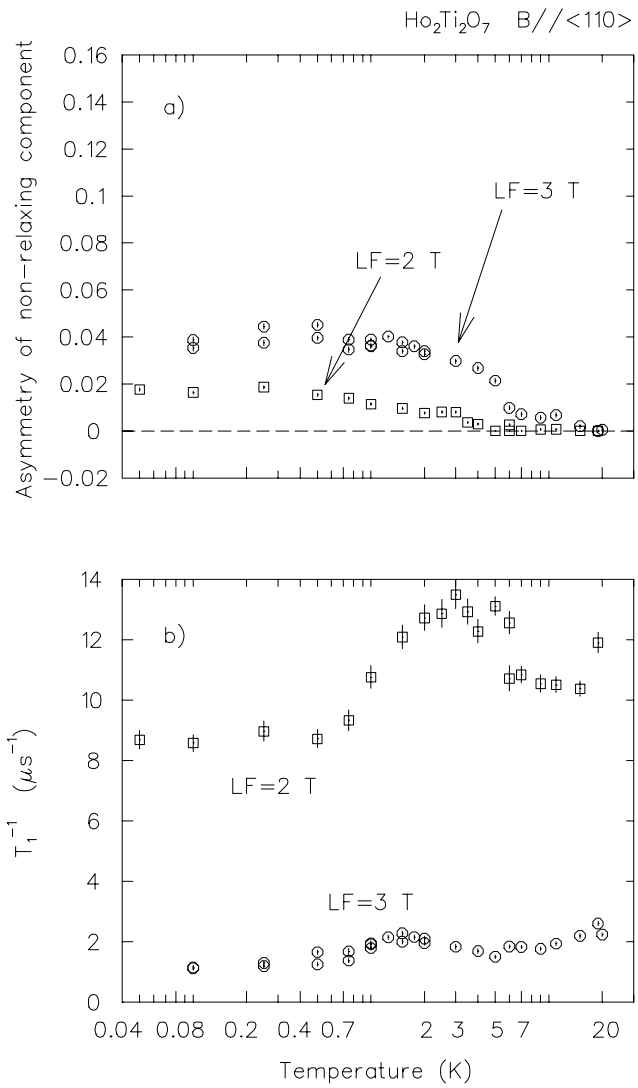

Fig. 100. a) Asymmetry of non-relaxing component and b) relaxation rate of muon spin polarization in $Ho_2Ti_2O_7$ as a function of temperature.

$Ho_2Ti_2O_7$ ($H \parallel \langle 110 \rangle$)

In this case half of the Ho spins lie perpendicular to the applied field and are thus unaffected by it. As shown in Figs. 100 and 101, the amplitude of the non-relaxing component is smaller in this orientation. The broad peak in $1/T_1$ observed at ∼1.5 K may be associated with the $\mathbf{q} = X$ ordered phase seen by inelastic neutron scattering [Harris *et al.*, Phys. Rev. Lett. *op. cit.*]. Once again, significant dynamics persist within the spin ice regime; an unexpected result.

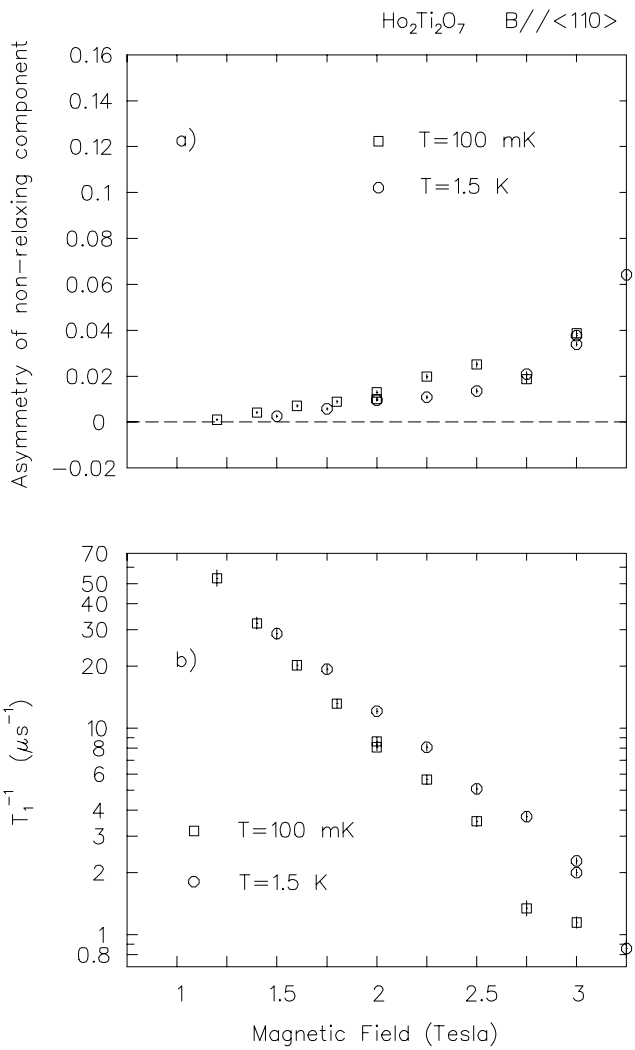

Fig. 101. a) Asymmetry of non-relaxing component and b) relaxation rate of muon spin polarization in $Ho_2Ti_2O_7$ as a function of applied magnetic field.

Experiment 860
Mass and charge transport in disordered media: orientational glasses

(J.H. Brewer, UBC; V.G. Storchak, Kurchatov Inst.)

Electron localization by orientational disorder in solid N_2-Ar mixtures

Electron transport in metals is known to be strongly affected by disorder, a dramatic example being "Anderson localization" where sufficiently strong disorder causes spatial localization of electron states near the Fermi level and thus drives the Anderson transition to an insulating state. However, the electron-electron interactions in metals dramatically modify the density of states at the Fermi level, leading to formation of the Coulomb pseudogap. To observe the effects of disorder on electron transport without the complications of electron-electron interactions, one must therefore study electron dynamics in a disordered insulating host.

A special class of solids formed by random mixtures of molecular and atomic species offers a unique opportunity for such studies. Pure molecular crystals like solid N_2 or CH_4 undergo an order-disorder phase transition from the "plastic crystal" high temperature phase (where the multipole moments associated with the molecules can rotate more or less freely) to a low temperature phase with long-range orientational order. This order is severely frustrated by the random substitution of spherical atoms or molecules (e.g. Ar in N_2, Kr in CH_4 or para-H_2 in ortho-H_2 etc.); strong enough dilution generally leads to a new type of phase called an orientational glass in which the multipole moments are "frozen" in random directions [Hochli, Knorr and Loidl, Adv. Phys. **39**, 405 (1990)]. One of the best studied orientational glass systems is the N_2-Ar mixture. Pure N_2 has two low-pressure crystalline forms, the low temperature orientationally ordered *fcc* α phase for $T < T_{\alpha\beta} = 35.6$ K and the high temperature orientationally disordered *hcp* β phase for $T > T_{\alpha\beta}$. Since N_2 and Ar are completely miscible, solid $(N_2)_{1-x}Ar_x$ is obtained by simply cooling liquid mixtures. The *hcp* sites are randomly occupied by N_2 and Ar. As the Ar concentration x is increased, $T_{\alpha\beta}$ decreases until for $x > x_c \approx 0.23$ the *hcp* lattice is stable to $T = 0$. The dynamical orientational disorder of the high-T phase eventually freezes into a static pattern of randomly oriented N_2 molecules, the orientational glass [Hamida, Genio and Sullivan, J. Low Temp. Phys. **103**, 49 (1996)]. One can gradually change the local order parameter and even switch the disorder on and off by changing the temperature and/or Ar concentration. These features make N_2-Ar mixtures very convenient systems for studying the effect of disorder on electron transport, especially since the orientational degrees of freedom are strongly coupled to lattice displacements: reorientation of a multipole moment involves changes of atomic coordinates. Because of this coupling, orientational glasses exhibit transport properties analogous to those of translational glasses like amorphous SiO_2.

Being a mixture of insulators, the N_2-Ar system has a very large energy gap (~10 eV), so that even at high temperature the ambient density of free electronic states is exponentially low. Experimental study of electron transport in this system therefore requires that the empty conduction band be "injected" with free carriers, ideally in low enough concentrations that electron-electron interactions can be safely ignored. The ionization of molecules and/or atoms by high energy charged particles (e.g. positive muons) offers just such a source of free carriers.

Recent μ^+SR experiments [Storchak *et al.*, Phys. Lett. **A193**, 199 (1994); Phys. Rev. Lett. **72**, 3056 (1994); Phys. Rev. Lett. **75**, 2384 (1995); Phys. Rev. Lett. **76**, 2969 (1996); Phys. Rev. Lett. **78**, 2835 (1997); Appl. Mag. Reson. **13**, 15 (1997); Rev. Mod. Phys. **70**, 929 (1998); Phys. Rev. **B59**, 10559 (1999); Eshchenko, Storchak and Morris, Phys. Lett. **A264**, 226 (1999)] in liquid and solid nitrogen as well as liquid and solid neon and argon [see also 1997 TRIUMF Annual Report, Expt. 775] have shown that the spatial distribution of these ionization-track products is highly anisotropic with respect to the final position of the muon: the μ^+ generally thermalizes well "downstream" from the last ionization event where an excess electron was generated, and that electron is often mobile enough to reach the thermalized muon and form muonium. This phenomenon of delayed muonium formation (DMF) is very sensitive to the electron mobility – a free electron in the conduction band will quickly reach the μ^+, whereas an electron that undergoes localization to become a polaron will arrive much later, if at all. (Typical mobilities in insulators range from about $10^2 - 10^3$ cm^2/V.s for delocalized electrons, to about $10^{-3} - 10^{-2}$ cm^2/V.s for localized electrons.) Thus DMF forms the basis of a new technique for measurements of the electron mobility b_e in insulators and semiconductors on a microscopic scale: b_e can be estimated whenever one can measure both the characteristic time for Mu atom formation τ and the characteristic distance between the stopped muon and its last radiolysis electron R. The former is determined from the magnetic field dependence of the muonium signal amplitude and phase, using the coherence criterion for Mu formation. The latter is extracted from the dependence of the muonium formation probability on applied electric field – basically, a sufficiently high applied electric field will overcome the Coulomb attraction between the muon and electron. The characteristic distances involved are typically on the order of 10–100 nm; the characteristic times are less than 10^{-10} s for delocalized electrons and range to microseconds for localized electrons. In the simplest case of viscous motion the parameters obey $\tau = R^3\epsilon/3eb_e$, where e is the electron charge and ϵ is the dielectric constant of the medium.

The potential of the μ^+SR-DMF technique for electron mobility measurements in solids was first demonstrated for pure solid nitrogen. Excess electrons were found to be delocalized in α-N_2, which shows a long-range orientational order. We have now found evidence for strong electron localization due to orientational disorder induced by Ar impurities in the low temperature orientational glass phase of solid nitrogen-argon mixtures, which may serve as model systems for studying electron localization in the absence of electron-electron interactions, and thus shed light on electronic transport in less exotic insulators and semiconductors.

The experiments were performed on the M20 beam line at TRIUMF and on the EMU beam line of the ISIS Pulsed Muon Facility at the Rutherford Appleton Laboratory. In each experiment, mixtures of ultra high purity N_2 and Ar (less than 10^{-5} impurity content) were condensed from the gas phase into a liquid. At ISIS the sample cells were 25 mm in diameter and 5 mm thick; at TRIUMF, they were 18 mm in diameter and 4 mm thick. Solid samples were carefully grown from the liquid phase at a typical speed of about 5 mm/hr under a vertical temperature gradient of about 2 K across the cell. At both laboratories, positive muons of 28 MeV/c momentum and 100% spin polarization were stopped in the samples and μ^+SR time spectra were recorded at various temperatures and applied magnetic and electric fields. The muon decay asymmetry time spectrum $A(t)$ directly reveals the time-dependent amplitudes of the characteristic precession signals of paramagnetic (Mu) and diamagnetic (μ_D) species, both of which are present in all $(N_2)_{1-x}Ar_x$ mixtures studied.

The μ_D signal sometimes exhibits two components: one which is slowly damped due to random local fields from ^{14}N nuclear moments, and one which disappears much faster due to very delayed Mu formation. The latter is only observed in cases where the electrons form polarons which are still mobile enough to reach the μ^+ on a μs timescale. The general form of the μ^+SR asymmetry spectrum is therefore

$$\begin{aligned} A(t) &= A_{\rm Mu} e^{-\lambda_{\rm Mu} t} \cos(\omega_{\rm Mu} t + \phi_{\rm Mu}) \\ &+ A_{\rm S} e^{-\lambda_{\rm S} t} \cos(\omega_\mu t + \phi_{\rm D}) \\ &+ A_{\rm F} e^{-\lambda_{\rm F} t} \cos(\omega_\mu t + \phi_{\rm D}), \end{aligned}$$

where $A_{\rm Mu}$, $\phi_{\rm Mu}$ and $\lambda_{\rm Mu}$ are the amplitude, initial phase and relaxation rate for the muonium signal and the corresponding quantities with S and F subscripts parameterize the "slow" and "fast" decaying μ_D signals, which have a common initial phase $\phi_{\rm D}$. The sum $A_D = A_{\rm S} + A_{\rm F}$ defines the net diamagnetic asymmetry. Muonium relaxation is caused by its nuclear hyperfine interactions.

Figure 102 depicts the temperature dependences of the asymmetries (amplitudes) of the various signals in solid $(N_2)_{1-x}Ar_x$ for $x = 0$, 0.09, 0.16 and 0.25. At high temperature (above about 40 K), all the mixtures have roughly the same Mu and μ_D asymmetries as pure N_2. At low temperatures, however, adding argon causes dramatic changes. In pure N_2 below about 30 K there is a large Mu signal and a small μ_D signal, indicating efficient DMF; as Ar is added there is a progressively larger μ_D signal, indicating reduced DMF,

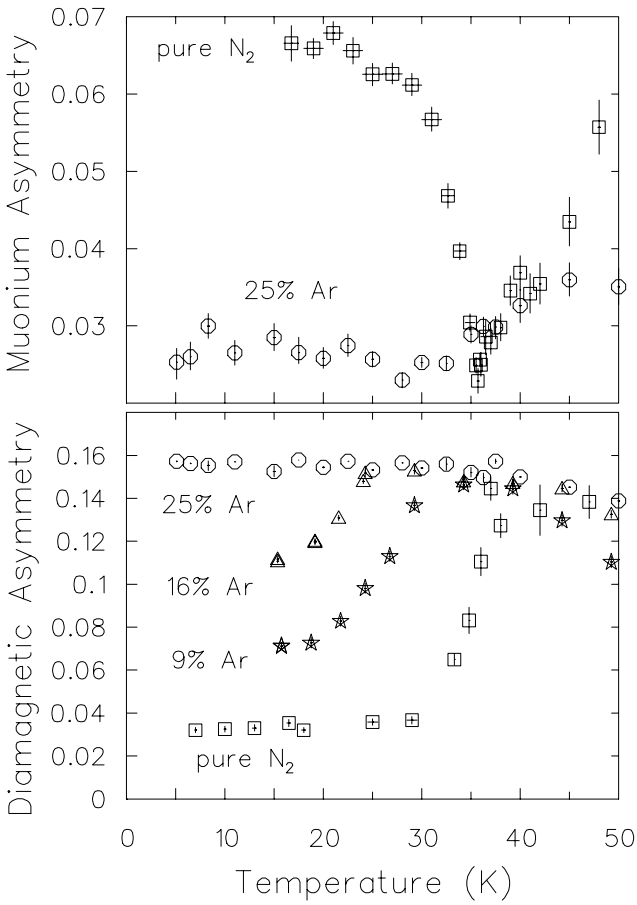

Fig. 102. Temperature dependences of muonium (top, $H \approx 5$ G) and net diamagnetic (bottom, $H \approx 100$ G) signal amplitudes in pure solid nitrogen (squares) and solid $(N_2)_{1-x}Ar_x$ (circles: $x = 0.25$; triangles: $x = 0.16$; stars: $x = 0.09$).

until at $x = 0.25$ there is only a small Mu signal. The increase in Mu amplitude is only half the corresponding decrease in μ_D amplitude because half the Mu polarization oscillates at the muonium hyperfine frequency and appears depolarized. Full asymmetry is about 0.19 in these experiments.

In solid N_2, we have shown that muonium formation proceeds via two channels: the thermal DMF process outlined above and the epithermal prompt process which takes place prior to the μ^+ thermalization and is therefore independent of temperature, electron mobility, etc. The small, temperature independent Mu amplitude in the $x = 0.25$ sample (see Fig. 102) is the same as the prompt Mu amplitude in pure solid nitrogen, suggesting a complete absence of DMF in the orientational glass.

The hypothesis that Mu formation in the $x = 0.25$ mixture is essentially all via the prompt (epithermal) channel at 20 K is further supported by the observation that $A_{\rm Mu}$ and A_D do not depend on an externally

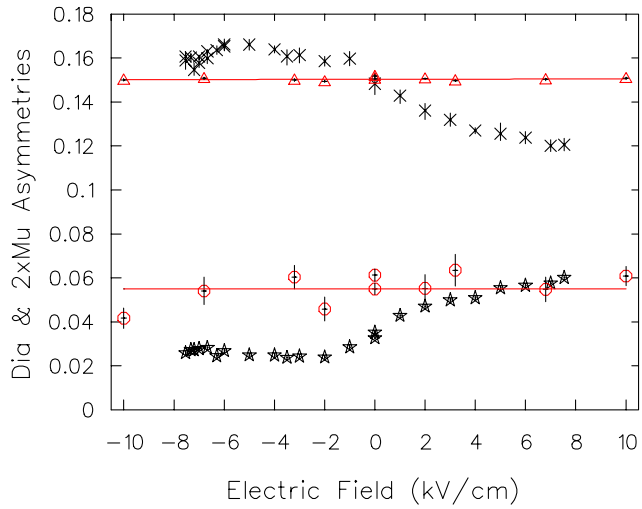

Fig. 103. Electric field dependences of $2 \times A_{\rm Mu}$ and A_D in pure solid nitrogen (crosses and stars, respectively) and in solid 75% N_2 + 25% Ar (circles and triangles, respectively) in a transverse magnetic field $H = 36$ G at $T = 20$ K. The muonium amplitudes are doubled to compensate for the 50% depolarization of Mu by hyperfine oscillations.

applied electric field for that sample, as shown in Fig. 103. Both amplitudes show significant electric field dependence in pure N_2 at 20 K, from which the characteristic muon-electron distance R is estimated to be about 50 nm; about the same value of R is found in solid Ar, which exhibits almost 100% DMF. The fact that solid N_2 and solid Ar have similar values of R is not at all surprising, since N_2 molecules and Ar atoms have about the same size and about the same ionization potential [see *Cryocrystals*, Verkin and Prikhotko, eds. (Naukova Dumka, Kiev, 1983)] and therefore about the same cross section for muon (or Mu atom) scattering. It is therefore natural to expect that R is about the same in mixtures as in the pure substances. The absence of DMF at this length scale at low temperature in the $x = 0.25$ mixture suggests that electrons are localized in this orientational glass.

One might suspect that it is the difference between lattice sites randomly occupied by N_2 molecules and Ar atoms which acts as a localizing influence, for example by simple scattering (or even trapping) of initially delocalized electrons by Ar impurities. However, Fig. 102 shows that mixtures without sufficient Ar concentrations to destroy orientational order at low temperature still exhibit efficient DMF; this process requires delocalized electrons. Scattering of these electrons by Ar impurities is unlikely to depend qualitatively on whether the 12 nearest neighbours of a typical lattice site include 1 Ar atom ($x = 0.09$), 2 Ar atoms ($x = 0.16$) or 3 Ar atoms ($x = 0.25$). Evidently the electrons are localized only by an Ar concentration of 0.25 or greater – i.e. in the glassy phase.

Experiment 876
Disordered magnetism near magnetic instabilities in *f*-electron materials
(D.R. Noakes, Virginia State)

This is an experiment to measure ZF and LF-μSR in three types of f-moment material: UPdSn, $U_{1-x}Y_xCoAl$, and $PrAu_2(Si_{1-x}Ge_x)_2$. In the first week of beam in October, powder samples of UPdSn, $PrAu_2Si_2$, $PrAu_2Ge_2$, and $PrAu_2(Si_{0.8}Ge_{0.2})_2$ were measured at M20.

Study of UPdSn extends μSR work by members of this collaboration on CeTSn materials (T = Ni, Cu, Pd, Pt) to a uranium 1:1:1 analogue. Among the 1:1:1's, the uranium moments in UPdSn seem more stable than usual, entering a long-range ordered magnetic state at a relatively high 37 K. A second transition at 25 K, however, has been interpreted as due to ordering of a component of the uranium moment left disordered in the 37 K ordering. We want to use μSR to directly probe for this disordered component within the ordered state, which so far has been deduced only indirectly.

$PrAu_2Si_2$ is a spin glass that provides a foil for URh_2Ge_2, the latter a heavy fermion system previously thought to be the only stoichiometric spin glass among the large number of known 1:2:2 materials. We want to measure the spin dynamics above $T_g \simeq 3$ K, and the development of the frozen state below this. Further, we proposed to measure μSR in $PrAu_2Ge_2$ and $PrAu_2(Si_{0.8}Ge_{0.2})_2$, to determine whether the spin glass state for $x < 0.2$ in $PrAu_2(Si_{1-x}Ge_x)_2$ can be related to the antiferromagnetic state for $x \geq 0.2$.

UPdSn

This radioactive powder was immobilized in stycast plastic. From 70 K down to 50 K in ZF, there is slow exponential relaxation, with rate increasing slightly as temperature decreases. At 45 K and 42 K, a fast-relaxing signal develops in the early bins and, at 40 K, a spontaneous oscillation frequency near 12.5 MHz is resolved. While the Néel temperature is usually placed between 35 K and 40 K (sample and probe dependent), in all neutron scattering reports [Robinson *et al.*, Phys. Rev. **B45**, 2939 (1992); J. Appl. Phys. **75**, 6589 (1994)] magnetic Bragg peaks, apparently resolution limited, are always reported up to about 43 K. The transition temperature for the neutron experiments has been interpreted as the point of maximum slope on a plot of intensity versus temperature, where the curvature switches from concave-up to concave-down (Brillouin-like). The non-Brillouin-like behaviour immediately below 43 K is reasonably interpreted as inhomogeneous freezing, not critical behaviour. Supporting this, the slow-relaxing asymmetry in our measurements starts dropping as the temperature falls below 45 K, and the oscillating signal asymmetry rises below 40 K, stabilizing at 35 K and below. The relaxation rate of the oscillating signal decreases with temperature. Between 26 K and 22 K, a two-frequency pattern is observed, with a higher frequency signal increasing in amplitude at the expense of the lower-frequency signal of higher temperatures. An example spectrum is shown in Fig. 104.

Below 22 K, only the higher-frequency signal is seen. Thus we see an ≈4 K range of inhomogeneous reordering. The temperature dependence of the observed frequencies is shown in Fig. 105.

Normally, the spontaneous oscillation frequency is proportional to the magnetic order parameter (sublattice magnetization), and so it would normally decrease as the temperature is raised toward the ordering temperature. In Fig. 105, the higher frequency

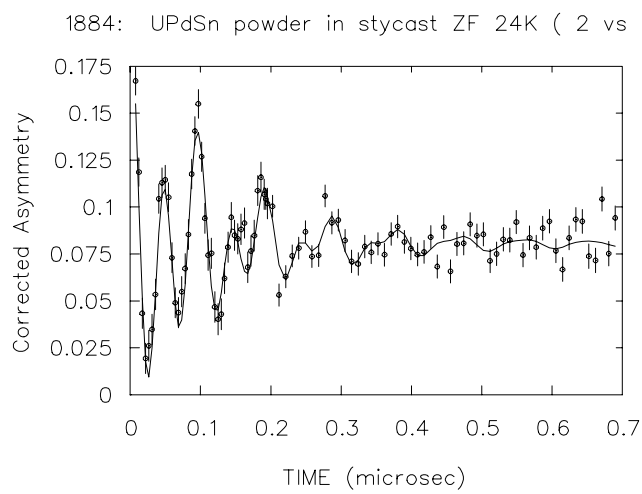

Fig. 104. ZF-μSR asymmetry spectrum of UPdSn at 24.0 K. The solid line shows a least-squares fit of a two-frequency model.

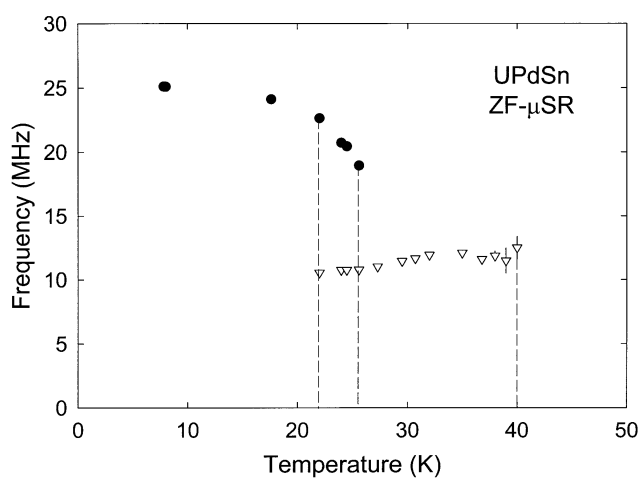

Fig. 105. Temperature dependence of the spontaneous oscillation frequencies observed in ZF-μSR of UPdSn. The dashed lines indicate 22 K, 25.6 K and 40 K.

corresponding to the lower-temperature ordered state conforms to this expectation, but it is clear that, in the higher-temperature ordered state, the frequency increases slightly with temperature. Neutron scattering results [Robinson *et al.*, J. Magn. & Magn. Mater. **128**, 143 (1993)] indicate that the ordering is complicated, with a non-collinear spin structure and a structural distortion at each transition, and that leaves scope for such μSR behaviour to occur.

In the paramagnetic state, UPdSn is hexagonal, as is CeCuSn (the other CeTSn materials we have studied are orthorhombic). It is interesting that our μSR studies of CeCuSn (Expt. 797) revealed similar behaviour in its "long-range ordered" signal [see Fig. 4 of Kalvius *et al.*, Physica **B289-290**, 252 (2000)], as shown in Fig. 106.

Less is understood about the magnetism of CeCuSn than UPdSn (no neutron scattering results have been published, for example), and there are substantial differences in their μSR behaviour. In CeCuSn, part of the sample volume enters a short-range ordered or spin-glassy state (this may be generating a higher-frequency oscillation, but the relaxation rate is so large that it is hard to be sure), associated with a heat capacity peak at 8.5 K. Then, at 7.4 K, the rest of the sample volume enters the long-range ordered state generating the frequency shown in Fig. 106, but the magnetism remains inhomogeneous to the low-temperature limit of our apparatus at the time, 2.0 K. The similarity of Fig. 106 and the lower frequency in Fig. 105 suggests that the long-range ordered fraction of CeCuSn has the same sort of spin structure as UPdSn.

$PrAu_2Ge_2$

We begin with this material because its behaviour is the most straightforward among our samples in this alloy series. In the paramagnetic state, ZF-μSR spectra showed monotonic relaxation. The 30 G TF relaxation rate is proportional to $1/T$ from the highest temperature we measured (230 K) down to at least 14 K. Extending over such a wide temperature range, and not obviously diverging at the transition temperature, this is likely to be due, at least in part, to crystalline electric field (CEF) effects [Noakes *et al.*, Phys. Rev. **B35**, 6597 (1987)] at the Pr site. Between 12.4 K and 12 K, ZF coherent oscillation sets in. Figure 107 shows the temperature dependence of the frequency, which is much more of the expected form for simple spin ordering below a second-order transition.

There is also a monotonic relaxation signal that persists below 10 K. At all temperatures, the best fits to the monotonic relaxation did not have simple exponential but power-exponential relaxation

$$G_z(t) = \exp\left[-(rt)^p\right].$$

In the paramagnetic state, the power p is roughly constant between 0.8 and 0.9. As the temperature drops below 12 K, the monotonic signal's rate rises in a manner similar to that of the frequency shown in Fig. 107, towards apparent saturation near 5 μs^{-1}, and p drops to 0.5. Temperature-dependent power less than one in the equation is generally associated with dynamic, disordered, dense magnetic moments, but there is little detailed understanding. The monotonic signal below 12 K is of approximately the same amplitude as the oscillating signal, and so is too large to be just the "1/3 tail" of the ZF spontaneous oscillation. It will require considerable careful analysis to separate the extra signal from the "1/3 tail", which must be there, decide whether the extra signal is within the same volume as the oscillating signal or represents macroscopic inhomogeneity, and decide whether it indicates substantial moment dynamics far below the ordering temperature.

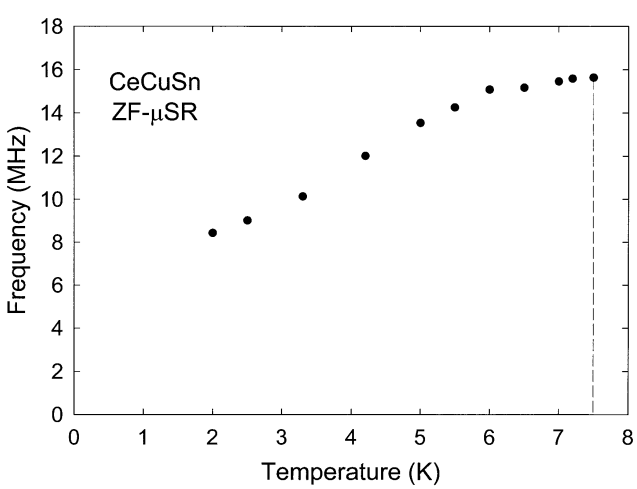

Fig. 106. Temperature dependence of the spontaneous oscillation frequency of the long-range ordered signal in ZF-μSR of CeCuSn. The dashed line indicates 7.4 K.

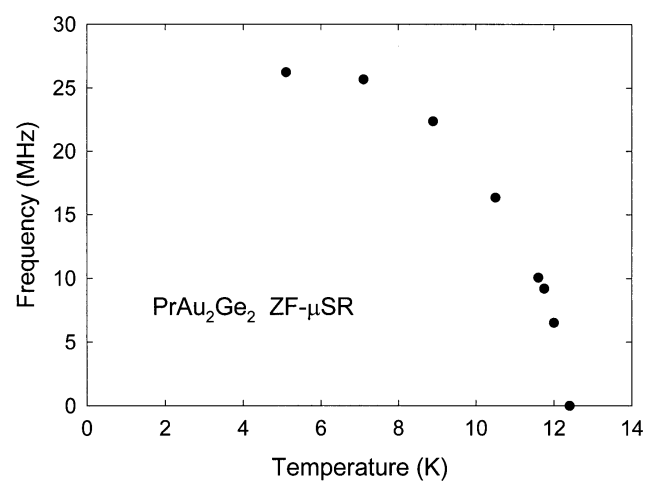

Fig. 107. Temperature dependence of the ZF-μSR spontaneous oscillation frequency in $PrAu_2Ge_2$.

With respect to the last, it may help to take LF-μSR data below 12 K to try to decouple the monotonic relaxation.

$PrAu_2Si_2$

In spite of the fact that this material is reported to spin-glass freeze at $\simeq$3 K, we saw only monotonic relaxation in ZF-μSR with the rate increasing as the temperature decreased, all the way down to 1.9 K, as low as this apparatus would take this sample. As with the previous sample, best fits to ZF data were obtained with the power exponential (see equation); in this case p dropping from 0.75 at 50 K to near 0.6 at low temperatures. As in the previous sample, the relaxation rate is proportional to $1/T$ over a wide temperature range. Rather than tending to diverge at any positive temperature, the rate below 4 K may be dropping slightly below $1/T$ dependence, which might, if we are lucky, be a very subtle indication that some spin freezing has begun. We need to measure this sample in the M15 dilution refrigerator to see if clear evidence of freezing develops well below 1.9 K.

$PrAu_2(Si_{0.8}Ge_{0.2})_2$

This sample showed monotonic relaxation at all temperatures down to near 5 K. At 5.0 K, there is a hint of a fast-relaxing signal. As the temperature drops further the fast-relaxing amplitude increases, indicating a range of inhomogeneous freezing, and at 4.0 K and below ZF spontaneous oscillation is resolved; roughly consistent with the reported Néel temperature. In this case we were able to coax the cryostat down to 1.7 K, producing the spectrum shown in Fig. 108.

We have only four spectra showing coherent oscillation, with the frequency rising from 14 MHz at 4.0 K to 24 MHz at 1.7 K. The zero-temperature limit frequency will be very similar to that of $PrAu_2Ge_2$ (Fig. 107), suggesting that the same type of ordered spin structure

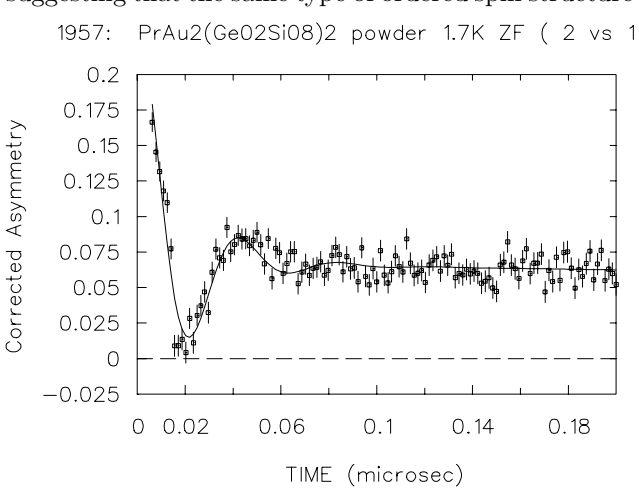

Fig. 108. ZF-μSR asymmetry spectrum of $PrAu_2(Si_{0.8}Ge_{0.2})_2$ at 1.7 K. The solid line is a least squares fit of a rapidly-relaxing oscillation.

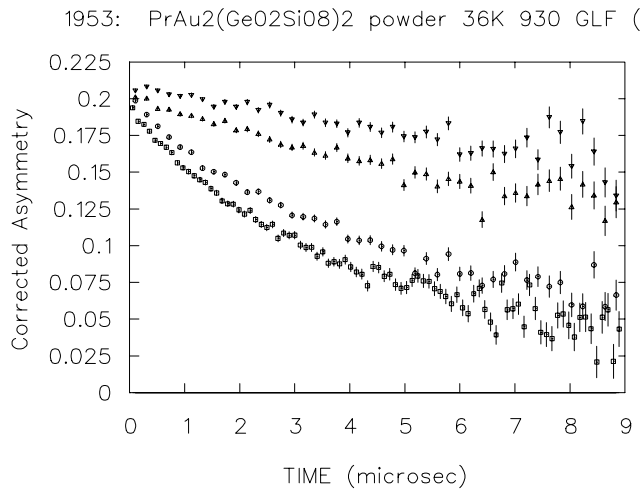

Fig. 109. μSR asymmetry spectra in $PrAu_2(Si_{0.8}Ge_{0.2})_2$ at 35 $\pm$ 1 K in ZF (squares) and longitudinal fields: 39 G (circles), 300 G (up triangles) and 930 G (down triangles).

develops, though with extra disorder induced by the non-magnetic site alloying, and also suggesting that the ordered moment at $T = 0$ is the same. The Si$\longleftrightarrow$Ge alloying reduces the transition temperature but not the ordered moment that develops, which is consistent with the introduction of frustration without reduction in the strength of the exchange coupling.

For this sample we attempted some LF decoupling and discovered, to our surprise, that not only could we decouple the ordered-state relaxation significantly with 3 kG LF, we could also decouple the paramagnetic relaxation at 35 K, as shown by Fig. 109.

Since we do not currently have a good physical model for the power-exponential form of the ZF spectrum, we have few grounds for expecting a standard model of LF decoupling to work here. Phenomenologically, the relaxation rate seems to go nearly as $1/\sqrt{B_{LF}}$, far from the standard $1/B_{LF}^2$. We should go back and check for paramagnetic LF decoupling in our end-point samples.

Experiment 882
μSR studies of unconventional superconductivity in an organic superconductor $(TMTSF)_2ClO_4$

(M.I. Larkin, Y.J. Uemura, Columbia)

Under Expt. 882 we have investigated the quasi-1 dimensional organic superconductor $(TMTSF)_2ClO_4$ using deuterated samples. Measurements of the upper-critical field H_{c2}, NMR relaxation rate and Knight shift, and sensitivity to non-magnetic impurities all suggest an unconventional (and possibly p-wave) pairing state of this and other Bechgaard Salt superconductors.

We have used zero applied field muon spin relaxation measurements (ZF-μSR) in an attempt to observe spontaneous magnetic fields below $T_c = 1.1$ K. Similar to the cases of μSR in UPt_3 and Sr_2RuO_4, such fields would indicate a superconducting state which breaks time reversal symmetry (TRS). We did not observe spontaneous fields, as shown in Fig. 110, but have an uncertainty in our measurement of ± 0.25 G, which is comparable to the $\sim$0.4 G spontaneous field seen in Sr_2RuO_4. Deuterated specimens were used in an attempt to minimize background nuclear dipole fields. The specimens, consisting of several hundred needle-like single crystals, were tiled onto a flat backing with the most conducting a-axis perpendicular to the direction of the initial muon polarization. It was not possible to align the other two crystal directions for the several hundred samples.

The material we used totalled 60 mg over $\sim$0.7 cm^2 surface area, which is near the lower limit of what may be measured in the dilution refrigerator at TRIUMF (or anywhere). Transverse field measurements (TF-μSR) indicated that the sample did enter the superconducting state, and that muons were stopping in the sample. TF-μSR may also be used to measure the superconducting penetration depth as a function of temperature. Such information is helpful in determining if gaps exist in the superconducting order parameter.

Further measurements will be performed using a larger quantity of material with aligned crystals. TF-μSR and ZF-μSR measurements will both be performed. Crystal alignment and increased sample mass would both represent substantial steps forward, and would allow us to garner much more information concerning this most interesting and exotic superconductor.

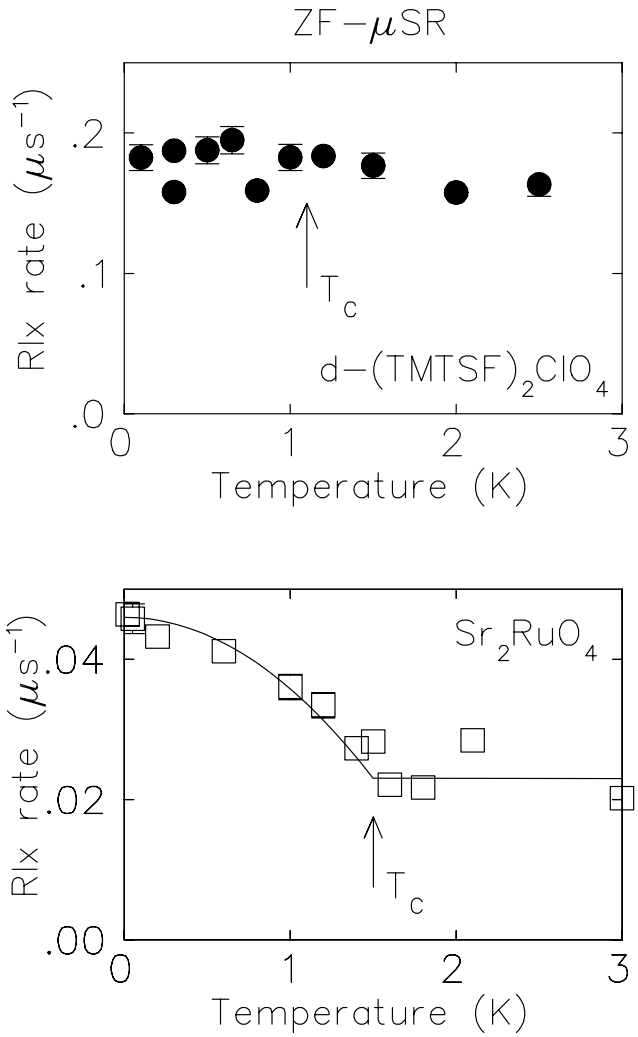

Fig. 110. ZF-μSR in deut-$(TMTSF)_2ClO_4$ and Sr_2RuO_4. No clear enhancement in relaxation is seen in deut-$(TMTSF)_2ClO_4$, in contrast to data from Sr_2RuO_4. Background nuclear dipole fields are fairly large in the TMTSF salt, however, possibly obscuring any effect.